SEDIMENTOLOGY the journal of the International Association of Sedimentologists

Sedimentology (2022) **69**, 1119–1150 doi: 10.1111/sed.12938

High-resolution facies analysis of a coastal sabkha in the eastern Gulf of Salwa (Qatar): A spatio-temporal reconstruction

MAX ENGEL* , CHRISTIAN J. STROHMENGER†,[1] , KIM T. PEIS‡, ANNA PINT‡,§, DOMINIK BRILL‡ and HELMUT BRÜCKNER‡

**Institute of Geography, Heidelberg University, Im Neuenheimer Feld 348, Heidelberg, 69120, Germany (E-mail: max.engel@uni-heidelberg.de)*

†ExxonMobil Research Qatar, Qatar Science and Technology Park, P.O. Box 22500, Doha, Qatar

‡Institute of Geography, University of Cologne, Zülpicher Str. 45, Cologne, 50674, Germany

§Institute of Geosciences, University of Jena, Burgweg 11, Jena, 07749, Germany

Associate Editor – Gregor Eberli

ABSTRACT

Sabkhas are key landforms along the southern coast of the Arabian Gulf and represent modern analogues for depositional and diagenetic processes controlling properties and quality of ancient hydrocarbon-bearing carbonates. While previous investigations of coastal sabkhas in Qatar have mainly focused on dolomitization processes, presented here is one of the first studies reconstructing facies changes and coastal formation in great detail. In the sabkha of Al-Kharayej (Gulf of Salwa), fifteen different facies types were distinguished based on twelve sediment cores, two trenches, as well as grain-size distribution, X-ray powder diffraction, thin section and microfossil analyses. Age estimates were based on seventy-eight ^{14}C-AMS and optically stimulated luminescence data. The sabkha parasequence comprises pre-transgressive dune sands, a thin, transgressive layer of reworked dune material, a mid-energy open-coast to open-lagoon facies, a low-energy lagoon facies, saline lake facies (salina: swallow-tail gypsum and gypsum mush) and the supratidal sabkha characterized by diagenetic overprinting (buckled gypsum crusts and halite crust). Transgressive marine flooding created open-coast to open-lagoon sedimentation after *ca* 7000 cal yr BP, followed by initial spit formation at the northern sabkha end at the beginning of the relative sea-level highstand (6000 cal yr BP). This main outer spit prograded southward and a more narrow, low-energy spit, diverted landward, closing a small lagoon in the northern sabkha 4500 to 4000 cal yr BP. The falling relative sea-level and longshore drift intensified the southward extension and widening of the main spit, and the main lagoon became more shallow. At 2000 to 1500 cal yr BP, the outer spit had almost closed the main lagoon, leading to salina and, finally, sabkha conditions. It is shown how specific local conditions (coastline orientation; wind, wave, tidal energy, longshore drift; depositional relief; sediment sources) created a spit-controlled sabkha that is genetically distinct from the classical model of shore-perpendicular accumulation of coarser sediment during high tides or storms.

[1]Present address: ExxonMobil Production Deutschland GmbH, Riethorst 12, Hannover, 30659, Germany

Keywords Arabian Gulf, carbonates, diagenetic overprinting, evaporites, Holocene, sabkha, salina.

INTRODUCTION

The term 'sabkha' is the Arabic expression for salt flat and includes all types of coastal and inland salt flats in arid environments prone to varying frequency and duration of inundation. Evaporite deposition prevails, either within the sediment or at the surface, in combination with clays, silts and sands. The salinity of groundwater in sabkhas may reach up to 600 g L^{-1}, where mostly Na^{+} and Mg^{2+} as ions, and Cl^{-} and $[SO_4]^{2-}$ result in the precipitation of gypsum and anhydrites (e.g. Alsharhan & Kendall, 2003; Al-Farraj, 2005; Al-Jaloud & Hussain, 2006). Sabkhas have extremely flat, salt-encrusted or gypsum-encrusted surfaces with elevation controlled by the top of the groundwater capillary fringe (Warren *et al.*, 1985). They are very common landforms along the protected southern shores of the Arabian Gulf (Evans *et al.*, 1969; Taylor & Illing, 1969; Barth, 1998; Al-Farraj, 2005; Alsharhan & Kendall, 2011; Evans, 2011; Strohmenger *et al.*, 2011; Billeaud *et al.*, 2014; Whitaker *et al.*, 2014; Strohmenger & Jameson, 2015, 2018; Brauchli *et al.*, 2016).

The common model for coastal sabkhas of the southern Arabian Gulf implies that they are continuously fed by highly saline seawater replacing evaporative losses in the supratidal through a hydraulic gradient, i.e. 'evaporite pumping' (Hsü & Siegenthaler, 1969) and, in many cases, gravitational replacement of groundwater by seawater during highest tides (Butler, 1969; McKenzie *et al.*, 1980; Barth, 1998). In the Abu Dhabi sabkhas, it has also been shown that the main source of water and solutes may derive from continental groundwater (Wood *et al.*, 2002). Sabkhas may prograde into lagoons forming behind barrier islands, as along the Abu Dhabi coast (Alsharhan & Kendall, 2011; Strohmenger *et al.*, 2011). However, the initial formation of sabkhas can also be related to longshore dynamics in prograding coastal settings, where spit formation and high sediment input lead to the formation of a gradually closing lagoon, which at some point is cut off from the sea, becoming a hypersaline salina (saline lake), later overprinted by sabkha-type interstitial evaporite deposition and surface crust formation (Purser, 1985; Homewood *et al.*, 2007; Mettraux *et al.*, 2011).

While previous investigations of coastal sabkhas of Qatar have mainly focused on dolomitization processes (e.g. Illing & Taylor, 1993; Whitaker *et al.*, 2014; Shalev *et al.*, 2021), this paper presents one of the first studies along the Qatari coast aiming at deciphering facies changes and coastal formation processes through time in detail. The studied record reflects environmental changes from a pre-Holocene to early Holocene terrestrial environment to shallow marine flooding during the mid-Holocene relative sea-level (RSL) highstand. This was followed by the closure of the lagoon triggering the formation of a salina and, finally, a coastal sabkha. The coastal sabkha of Al-Kharayej was chosen, as it represents the widest and best developed example along the eastern part of the shallow Gulf of Salwa.

Present day arid-climate coastal systems, like those of Qatar, provide analogues for depositional and diagenetic processes that control the quality of ancient reservoirs. Many major reservoirs in Qatar and the Middle East (for example, Permo-Triassic Khuff and Jurassic Arab formations) formed under conditions that are remarkably similar to those shaping the Qatari coastline today (e.g. Jameson *et al.*, 2009; Strohmenger & Jameson, 2015).

STUDY AREA

The Qatar peninsula represents an anticlinal structure of uplifted Tertiary limestones, dolomites, marls, chalks and shales protruding into the southern Arabian Gulf (Fig. 1). Sedimentation started in a shallow-marine shelf environment during the Palaeocene. These thick sequences are overlain by Lower and Middle Eocene carbonates (Dammam Formation), today covering 80% of Qatar's surface. They are intercalated by evaporites and were also deposited in shallow water, although clays within the Upper Dammam Formation indicate gradual subsidence and greater depths. Tectonic uplift and folding since the end of the Middle Eocene caused the emergence of Qatar, resulting in continental conditions and a lack of preserved sediments from the Upper Eocene and Oligocene (e.g. Al-Yousef,

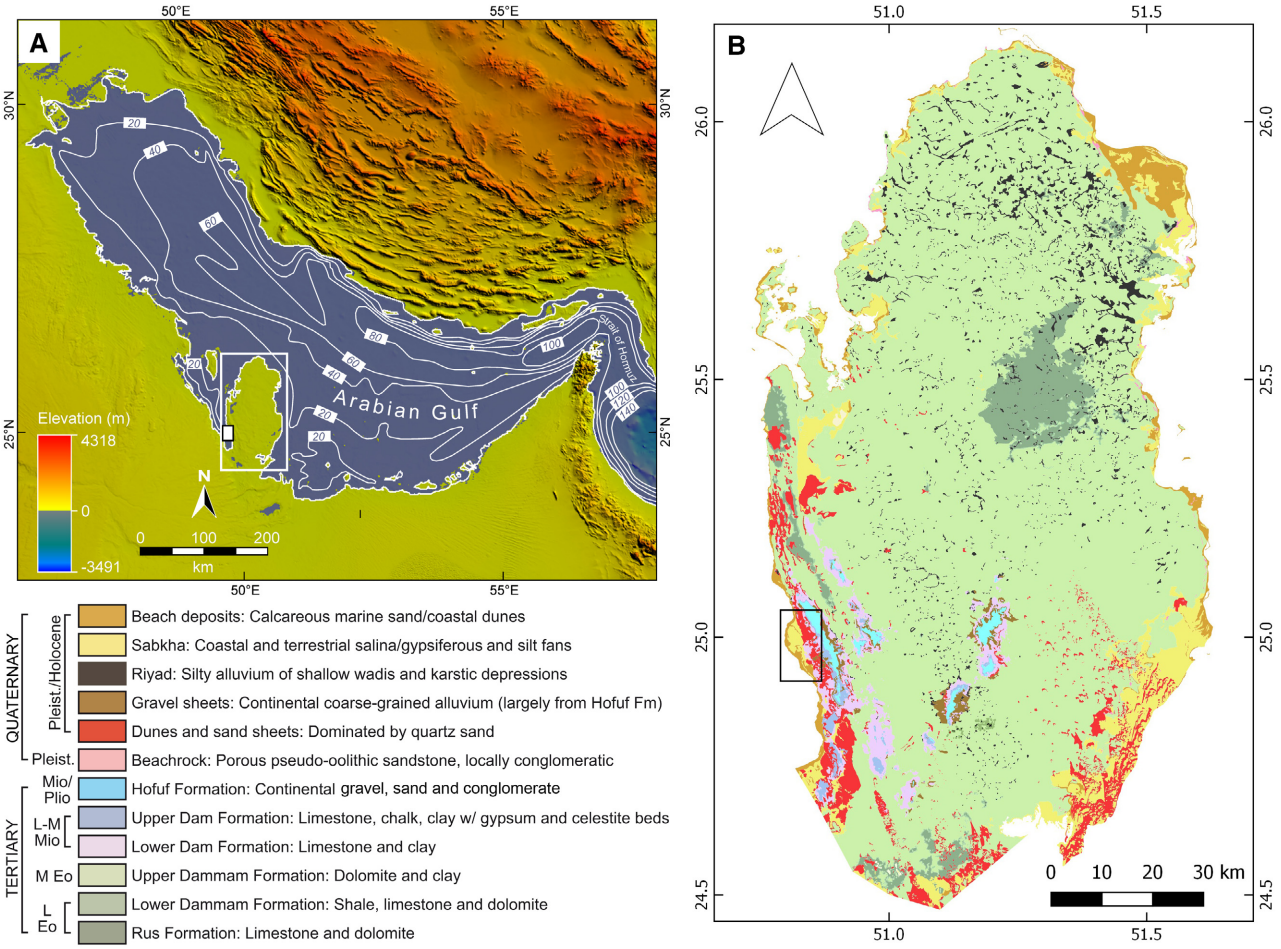

Fig. 1. (A) Topographic and bathymetric overview of the wider study region. Bathymetry and topography are based on the GEBCO_2014 grid (Weatherall *et al.*, 2015) and SRTM30 data (Farr *et al.*, 2007) provided by the US Geological Survey, respectively. The white frame indicates the extent of the map in Fig. 1B. (B) Geological map of southern Qatar based on the Qatar Geological Map of 1980 (State of Qatar, 1980). The black frame shows the location of maps in Fig. 2. L Eo, Lower Eocene; L-M Mio, Lower to Middle Miocene; M Eo, Middle Eocene; Mio/Plio, Miocene/Pliocene.

2003). Recently, Rivers & Larson (2018) and Rivers *et al.* (2019a) provided evidence for high-angle faulting underlying the roughly north–south-trending dominant structural landform of the Dukhan 'anticline', which, therefore, has been reinterpreted to be a reactivated graben system.

Miocene sedimentary rocks are mainly found in southern Qatar, represented by the shallow marine Dam and continental Hofuf formations. Quaternary deposits and landforms mainly comprise aeolian sand as sheets or barchan dunes (Embabi & Ashour, 1993; Engel *et al.*, 2018), silt to coarser-grained alluvium covering inland karst depressions (*riyad*) (Engel *et al.*, 2020), mixed siliciclastic–carbonate inland and coastal sabkhas (e.g. Al-Yousef, 2003; Billeaud *et al.*, 2014; Whitaker *et al.*, 2014; Strohmenger & Jameson, 2015, 2018), as well as skeletal beach sands (Shinn, 1973a; Strohmenger & Jameson, 2015; Rivers *et al.*, 2020).

The Arabian Gulf is a semi-enclosed, shallow sea with an average depth of 35 m (Fig. 1A). During the Last Glacial Maximum (LGM), global sea-level was about 120 to 130 m lower than today (Sarnthein, 1972; Kassler, 1973; Lambeck, 1996; Lambeck *et al.*, 2014) and the Arabian Gulf was dry until 14 000 years BP, with an ancient Shatt Al-Arab river feeding two separate freshwater lakes (Lambeck, 1996). After flooding, current sea-level was reached *ca* 7000 to 6500 years ago (Lambeck, 1996; Engel & Brückner, 2014; Strohmenger & Jameson, 2015; Parker

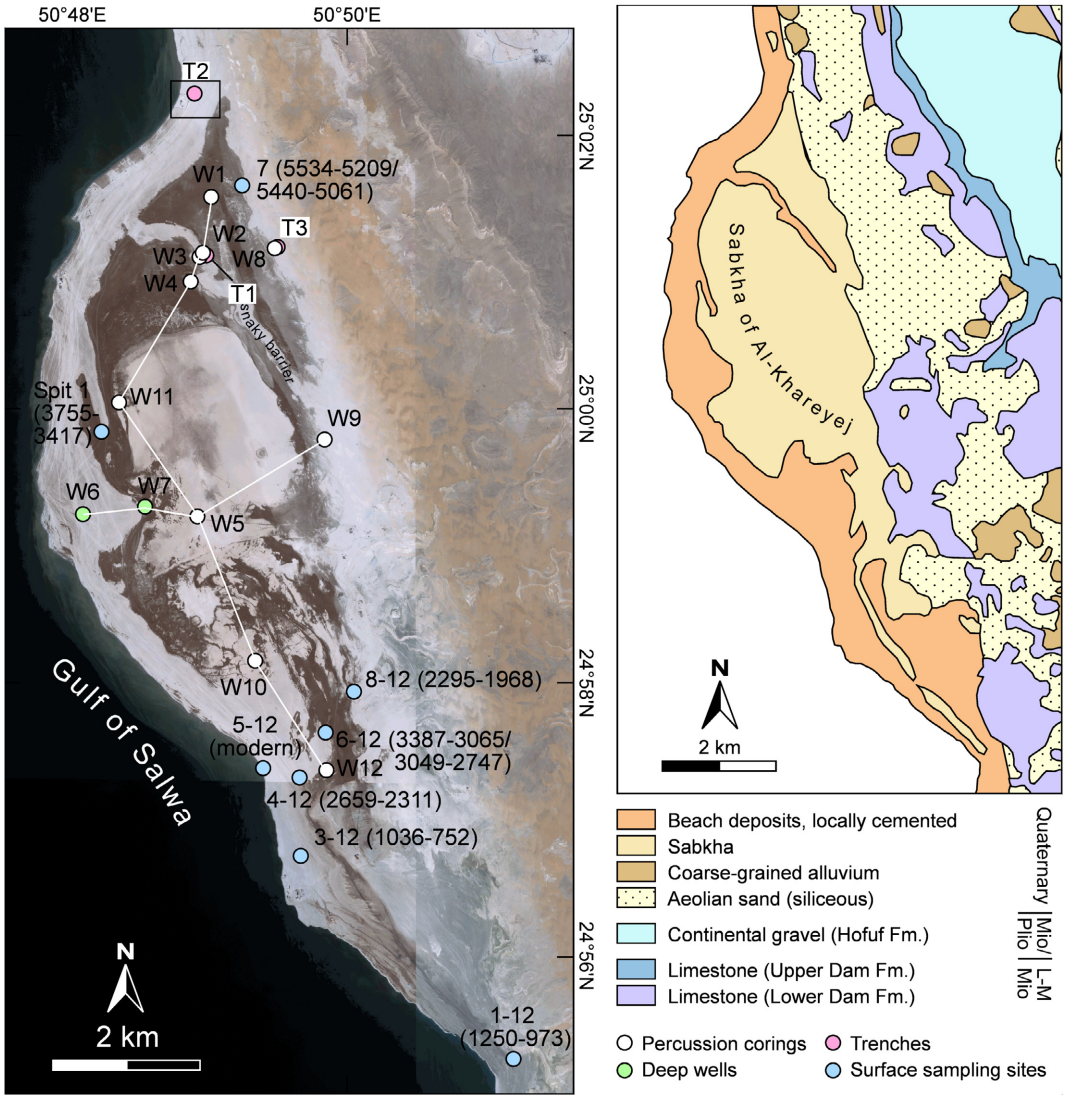

Fig. 2. Overview of the sabkha of Al-Kharayej, south-west Qatar, with location of sediment cores, deep wells, trenches and surface age dating sites with calibrated ^{14}C data (cal yr BP). The black frame around T2 indicates the map location of Fig. 12. White lines indicate the north–south (Fig. 3) and west–east (Fig. 4) transects. L-M Mio, Lower to Middle Miocene; Mio/Plio, Miocene/Pliocene. Satellite image: WorldView 2 from 2011; geological map based on Seltrust Engineering Ltd (1980).

et al., 2020). A RSL highstand of at least 2 m at around 6000 to 4500 years ago is indicated by stranded beach ridges, tidal channels and elevated sabkha deposits, for example, along the coastlines of Qatar, the United Arab Emirates (UAE) and Saudi Arabia (Strohmenger *et al.*, 2011; Engel & Brückner, 2014; Strohmenger & Jameson, 2018; Parker *et al.*, 2020). Regression since then induced shoreline migration of up to several kilometres in Qatar, for which, however, detailed, field-based spatio-temporal data are scarce (Cuttler & Al-Naimi, 2013; Billeaud *et al.*, 2014; Engel & Brückner, 2014; Strohmenger & Jameson, 2018).

The study site at Al-Kharayej protrudes into the Gulf of Salwa (Fig. 2), which is a very shallow extension of the Arabian Gulf, 110 km long and only 11 km wide at its southern end (Fig. 1A). It results from Quaternary tectonic subsidence (Kassler, 1973). The water depth is mostly <20 m (Fig. 1A). The tidal range is 30 cm for Dukhan, north-east Gulf of Salwa (State of Qatar, 2009), and water temperatures range between 20 to 35°C. The salinity increases

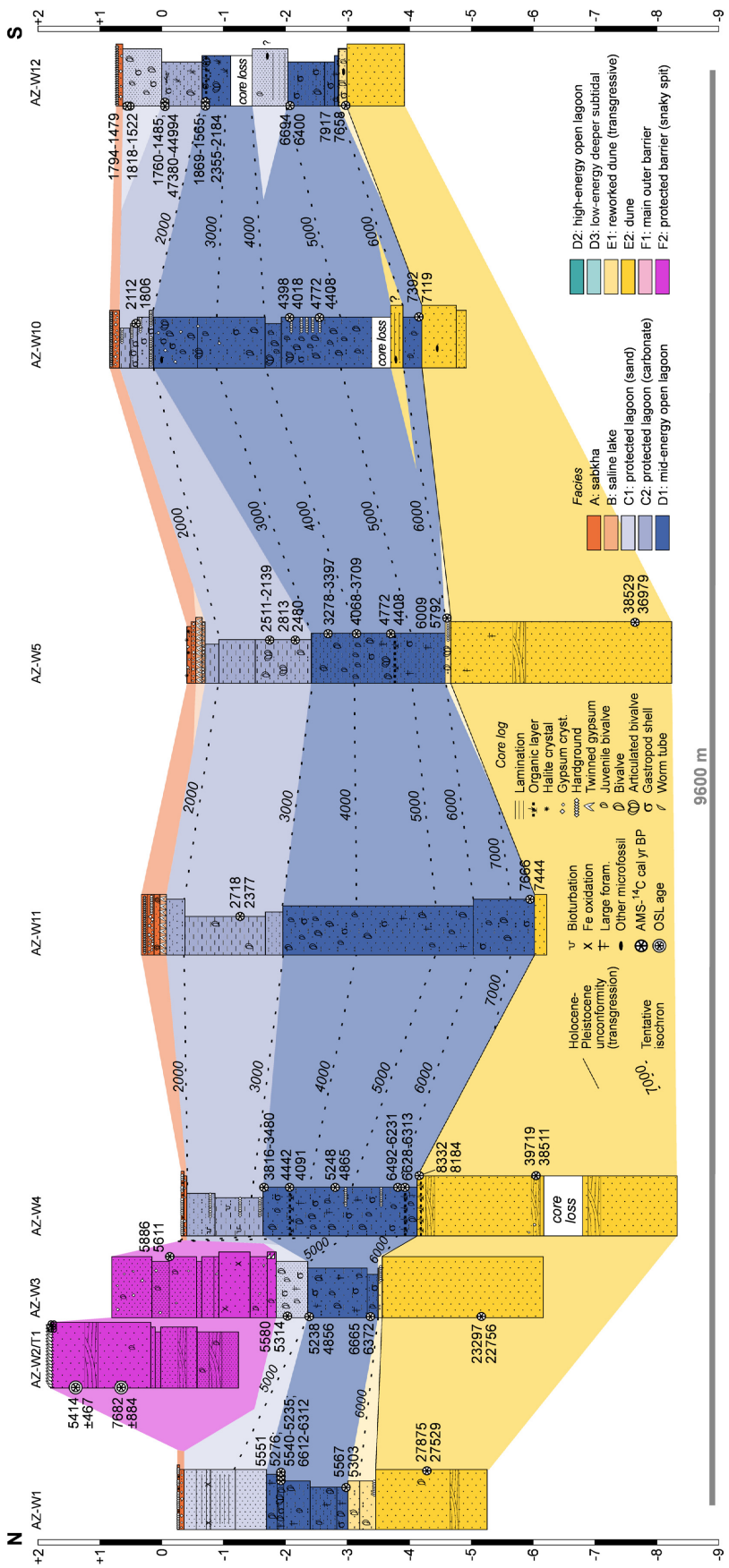

Fig. 3. North–south transect through the sabkha of Al-Kharayej (location in Fig. 2) showing facies distribution and calibrated age data (Tables S1 and S3). Sedimentary and microfossil data that led to the differentiation of facies are presented in Figs 5 to 7, 9 and 11).

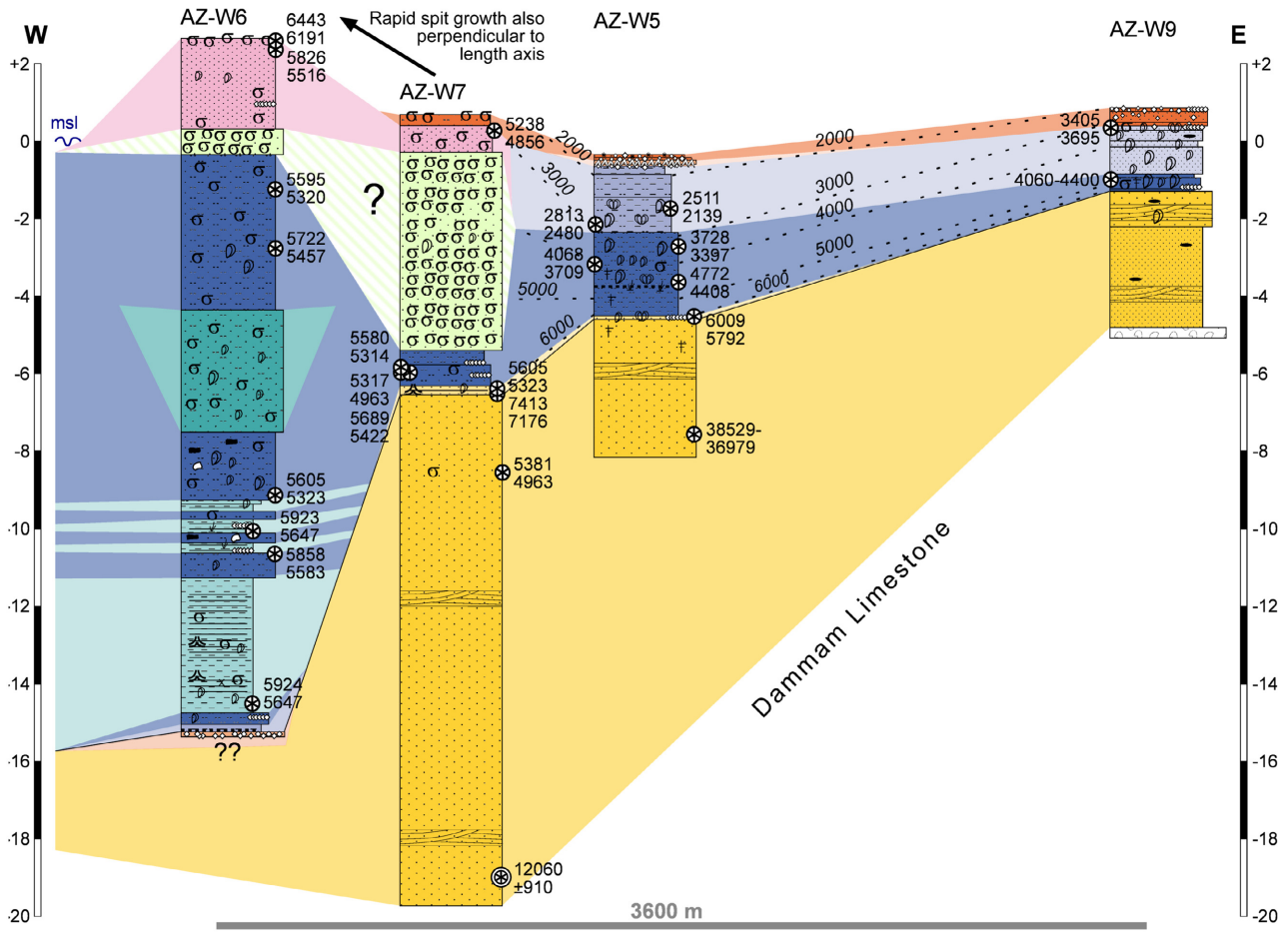

Fig. 4. West–east transect through the central part of the sabkha of Al-Kharayej (location in Fig. 2) showing facies distribution and calibrated age data (Tables S1 and S3). A legend to the core logs can be found in Figs 3 and 5. Sedimentary and microfossil data that led to the differentiation of facies are presented in Figs 5 to 7, 9 and 11).

towards the southern end (Sugden, 1963), ranging between 50 to 60 psu (Rivers *et al.*, 2019b), and partially up to 70 psu (Purser & Seibold, 1973; Sheppard *et al.*, 2010). The dominant regional Shamal wind system operating in a NNW–SSE direction (Rao *et al.*, 2001; Engel *et al.*, 2018) drives a moderate southward longshore drift at both sides of the Gulf of Salwa (Chao *et al.*, 1992).

METHODS

Ten vibracores up to a length of 8 m (AZ-W1 to AZ-W5; AZ-W8 to AZ-W12) were taken across the entire sabkha; they were documented and sampled in the field. Two wells with a diameter of 10 cm, up to 20.5 m deep, were drilled (AZ-W6 and AZ-W7) by Gulf Laboratories Co., Doha, Qatar, using a truck-mounted drill rig. Furthermore, two trench profiles were analyzed. All sampling sites were located using a digital global navigation satellite system (DGNSS).

The reconstruction of sedimentary environments and processes is mainly based on grain size (laser diffraction; high-speed camera), X-ray powder diffraction (XRD), thin section and microfossil analyses (foraminifera, ostracods). Grain-size data were analyzed with univariate statistical measures using GRADISTAT (Blott & Pye, 2001), and for data from cores AZ-W1 to AZ-W5 by end-member modelling using the R package EMMAgeo (Dietze & Dietze, 2019). The XRD and microfossil data were analyzed qualitatively and by principal component analysis (PCA) (Past 3.11 software; Hammer *et al.*, 2001). Age data were derived from 78 ^{14}C-AMS and optically

Table 1. Summary of the facies model. See also the stratigraphic profiles and proxy data (Figs 5, 7, 9, 11 and 13), thin section photographs (Fig. 6) and the photographic documentation from the field (Figs 8, 10, 15, S2, S5 and S6) for details on facies characteristics.

Facies	Lithology	Grain size	Macrofossils	Microfossils	Bedding	Hardground	Sedimentary environment
A	Mudstone/wackestone: strongly varying ratio of quartz grains (partly gypsum-encrusted and halite-encrusted) and lenticular and prismatic gypsum crystals	Fine to medium, medium to poorly sorted	Few poorly preserved cerithid shells and indeterminable mollusc fragments	–	–	Partly cemented crust at the surface (buckled gypsum crust on top, salt polygons in the centre)	Recent coastal sabkha, supratidal, diagenetic
B	Prismatic, twinned gypsum, minor occurrence of halite, aragonite, quartz	–	–	–	–	–	Saline lake, shallow subtidal to intertidal
C1	Mudstone/sandstone: quartz-dominated, carbonate material in minor amounts (peloids, skeletal grains, mollusc shells, some ooids), some millimetre-scale lenticular gypsum	Poorly sorted (due to skeletal grains)	Many well-preserved mollusc shells, bivalves in living position (e.g. *Hiatula mirbahensis*)	Abundance of foraminifera (*Peneroplis planatus, P. pertusus*) and ostracods (*Xestoleberis* spp., *Loxoconcha* spp.) varies	Non-bedded to bioturbated	–	Low-energy, protected lagoon, sand-dominated
C2	Aragonite mudstone to fine-grained peloid–skeletal packstone, partly aggregated by peloids: minor amounts of quartz grains, microbial lamination rare, ooids rare, various amounts of lenticular gypsum	Poorly sorted (due to skeletal grains)	Many mollusc shells (*Cerithium* sp.), bivalves in living position	Rich in foraminifera (*Quinqueloculina poeyana, P. planatus, P. pertusus, Ammonia tepida, Elphidium* spp.) and ostracods (*Xestoleberis* spp., *Cyprideis torosa, Loxoconcha* spp., *Keijella* spp., *Hemicytheridea* spp.)	Non-bedded to bioturbated	–	Low-energy, protected lagoon, carbonate-dominated
D1	Medium to coarse-grained skeletal–peloidal packstone to wackestone: rich in shell fragments,	Poorly to very poorly sorted	Many mollusc shells, some even articulated, large shell	Rich in foraminifera (*Q. poeyana, P. planatus, P. pertusus, A. tepida, Elphidium* spp.) and	Non-bedded to bioturbated	Intercalated hardgrounds or hardground clasts	Open lagoon, mid-energy shallow subtidal

Table 1. (continued)

Facies	Lithology	Grain size	Macrofossils	Microfossils	Bedding	Hardground	Sedimentary environment
	varying amount of carbonate mud (aragonite), minor amounts of quartz grains and ooids		fragments, rich in serpulids	ostracods (*Xestoleberis* spp., *Loxoconcha* spp., *Hiltermannicythere* spp.)			
D2	Coarse-grained grainstone with varying amount of very coarse skeletal debris: quartz grains, often carbonate-coated	Poorly to very poorly sorted	Larger mollusc shells and fragments	Minor amounts of foraminifera (*P. planatus, P. pertusus*) and ostracods	Non-bedded	Intercalated hardgrounds or hardground clasts	Open lagoon/open coast, high-energy shallow subtidal
D3	Fine-grained peloid–skeletal packstone: high amount of quartz grains, minor amount of clay minerals	Moderately to well sorted	Finer mollusc shells and fragments	Rich in foraminifera (*Q. poeyana*) and ostracods	Horizontally bedded (millimetre-scale)	Intercalated hardgrounds or hardground clasts	Low-energy, deeper subtidal
E1	Sandstone: quartz grains with minor carbonate coating, minor amounts of carbonate material (fine-crystalline dolomite, peloids, coated grains, skeletal grains)	Medium, moderately to well sorted	Very few shell fragments	–	Wavy bedded to non-bedded	Intercalated hardgrounds	Early Holocene transgression facies, reworked dune
E2	Sandstone: quartz grains, moderately to well-rounded, occasionally coated	Medium, well sorted	–	–	Low-angle cross-bedded to parallel bedded	–	Pre-Holocene aeolian dunes (sea-level lowstand facies)
F1	Skeletal–peloid grainstone: varying amounts of quartz, partly cemented (beachrock) with fenestral structures, pelagosite-type aragonite coatings	Medium to coarse, poorly to moderately sorted	Mollusc shells and large fragments (*Pinctada radiata*) concentrated in particular horizons	Not studied	Low-angle, cross-bedded, inclined seaward	Cemented as beachrock in some parts	Outer beach barrier: Mid-energy to high-energy foreshore environment, intertidal

Table 1. (continued)

Facies	Lithology	Grain size	Macrofossils	Microfossils	Bedding	Hardground	Sedimentary environment
F2	Sandstone: dominated by quartz grains, minor occurrence of skeletal carbonate, partly cemented (beachrock) with fenestral structures	Medium to coarse, moderately to well-sorted	Some cerithid and very few large bivalve shells	Some *Peneroplis* sp.	Low-angle cross-bedded to parallel bedded	Cemented as beachrock in some parts	Protected beach and beach spit: mid-energy foreshore, intertidal
G	Skeletal–peloid grainstone	Medium to coarse	Rich in mollusc shell fragments, few entire shells	Not studied	Cross-bedded, inclined landward	–	Backshore
H	Very coarse skeletal–peloid grainstone: dominated by massive shells	Very coarse, very poorly sorted	Rich in large mollusc shells (e.g. *P. radiata*) and shell fragments	Not studied	Low-angle seaward inclined onlap structures	–	High-energy foreshore
I	Grainstone with high amount of rounded to subrounded quartz grains	Medium to coarse, moderately to well-sorted	Few mollusc shells	Not studied	Cross-bedded to parallel bedded	–	Aeolian deposition in swales of the backshore
J1	Skeletal–peloid grainstone: varying amounts of quartz grains and coarse skeletal particles (occuring in pockets)	Medium to coarse, poorly sorted	Varying amount of mollusc shells and shell fragments, mostly concentrated in pockets	Not studied	Wavy bedding	–	Mid-energy upper shoreface

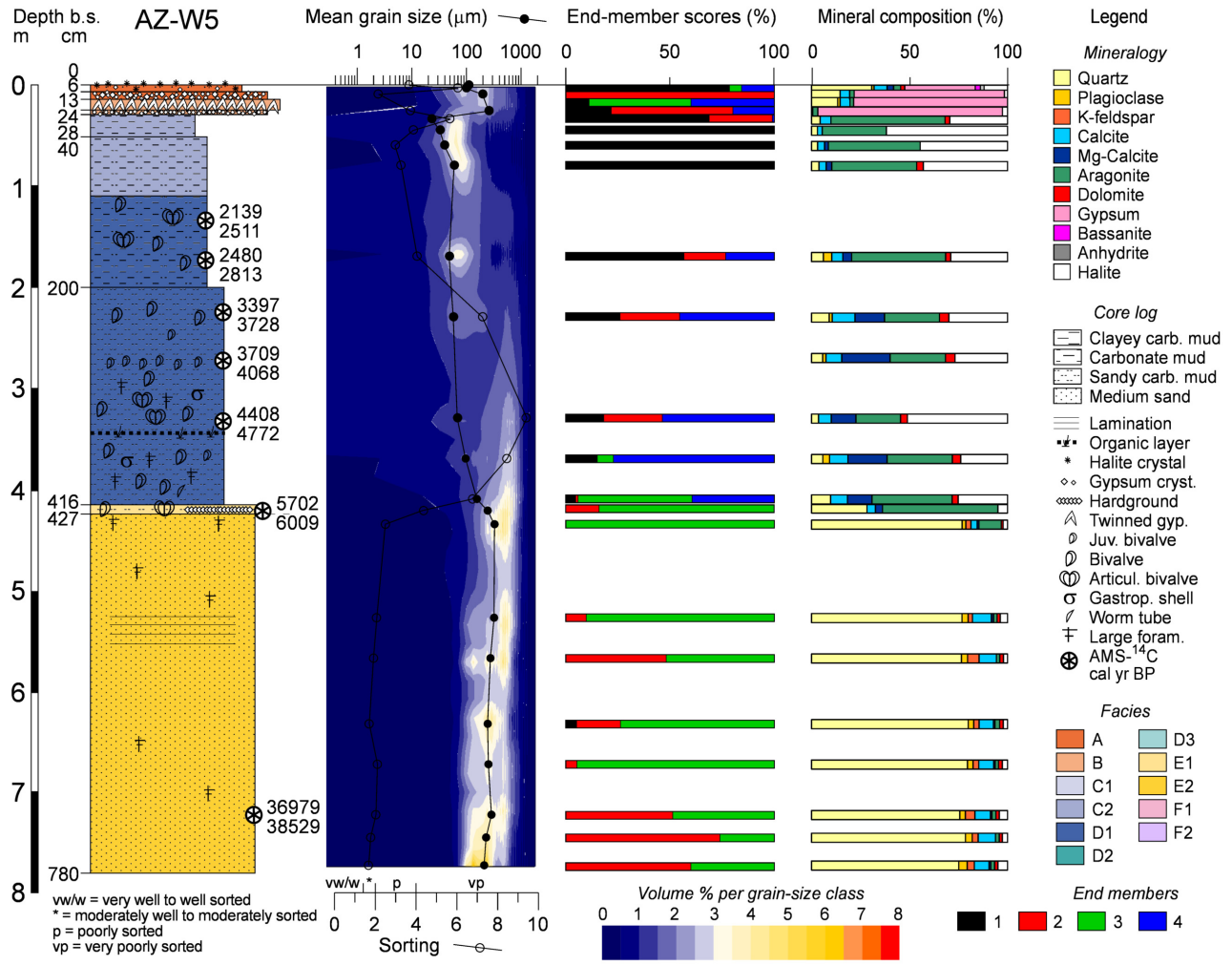

Fig. 5. Sediment core AZ-W5 (location in Fig. 2) with core log and data of particle-size distribution, end-member scores and mineralogy. Colours of end-member scores refer to the distribution of the four end members deciphered from the entire dataset AZ-W1 to AZ-W5 as shown in Fig. S3. The upper 40 cm of the stratigraphy are shown in detail on Fig. 8D.

stimulated luminescence (OSL) datings. All methodological details can be found in Appendix S1.

RESULTS

In total, 15 different facies types were identified in the study area, covering a wide range of texture and porosity. These facies types can be separated into those representing the sedimentary wedge underlying the modern sabkha (A, B, C1, C2, D1, D2, D3, E1, E2) and those forming the morphological barriers (F1, F2, G, H, I, J1). Their spatial distribution is indicated based on a north–south transect (Fig. 3) and an east–west transect (Fig. 4).

Facies types of the sedimentary wedge underlying the modern sabkha

The characteristics of all facies types are summarized in Table 1. Facies A occurs on top of all cores inside the sabkha (Figs 5, 6A and 7). It is usually cemented by a buckled gypsum crust, bassanite, anhydrite and, in the centre, halite. At the landward margins, this crust only very thinly covers the sand-dominated Facies C2 with articulated bivalves in living position indicating ongoing deflation. In the centre, where Facies A reaches a thickness of up to a few decimetres, surface structures comprise polygons (Fig. 8A), sometimes associated with characteristic tepee structures, and circular mounds created by

insular growth of large gypsum crystals (Fig. 8B and C). In the deep well AZ-W6, Facies A was also found at the base (Figs 9 and S2).

Facies B only occurs in the innermost part of the sabkha around core AZ-W5, where it underlies Facies A. It consists of a basal layer of almost pure millimetre-scale to centimetre-scale gypsum mush, partly cemented, confined by a massive layer of prismatic, twinned gypsum (swallow-tail gypsum), *ca* 10 cm in thickness (Figs 5 to 8D). The XRD reflects minor occurrences of halite, aragonite and quartz (Fig. 5).

Facies C1 (Figs 6D and 7) has a patchy occurrence, always underlying Facies A or B (or F2 in case of the inner barrier), with some bivalves of *Hiatula mirbahensis* in living position and exposed at the surface by deflation in the north near AZ-W1 (Fig. 10). C1 appears non-bedded and bioturbated, indicated by vertical burrows well-preserved in the weakly consolidated carbonate near AZ-W4 (Fig. 10A and B). Facies C2 (Figs 6E and 7) occurs throughout most of the sabkha, in a thickness of up to 2 m close to the surface. The particle-size distribution is fully represented by end member 1, the distribution of which is very broad, peaking at 100 μm (Fig. S3). Associations of foraminifera and ostracods are both more abundant and diverse compared to C1 (Fig. 11).

Facies D1 is the most common facies inside the sabkha, found at a depth of *ca* 1 to 4 m below the present sea-level (Figs 6F, 6G and 7). D1 is poorly sorted, best represented by the coarsest end member 4 with a main peak near 900 μm, a broad distribution and two smaller peaks close to 100 μm and <1 μm (Figs 5 and S3). Facies D2 (Figs 6I, 6H and 7) is only found in the deep core AZ-W6 from the outer barrier at a depth of 1010 to 700 cm b.s. (below surface) (Fig. 9). Facies D3 (Figs 6J and 7) is also only found in AZ-W6, where it occurs below D2 and alternates with D1 (Fig. 9).

Facies E1 (Fig 6K and 7) is typically thin and found in between D1 and E2. It is not identified in all cores. Minor amounts of carbonate comprise fine-crystalline rhombs of dolomite (Fig. S4). The particle-size distribution is best represented by unimodal end member 3 peaking in medium to coarse sand (Figs 5 and S3). Facies E2 (Figs 6L and 7) either underlies D1 or E1. It resembles E1, but lacks carbonate, apart from very few large but poorly preserved foraminiferal tests of *P. planatus* documented in the field, and occasional grain coatings. The particle-size distribution is almost equally represented by end members 2 and 3, the former showing two minor peaks in the clay category and at the silt/sand boundary in addition to the main one, which is shifted towards the fine/medium sand boundary (Figs 5 and S3). E2 represents the bottom facies in every core (Figs 3 and 4).

Facies types of the barriers

The sabkha comprises two different types of barriers with six different documented facies types (Table 1). The main barrier is up to 1 km wide, up to 2.5 m higher than the sabkha floor, and separates the sabkha from the Gulf of Salwa (Figs 2, 12 and 13). Another narrow barrier, only 250 m wide, up to 2 m higher than the sabkha floor, and with a snaky outline runs across the northern part of the sabkha from the outer barrier inland in a south-eastern direction, thereby constantly losing width (Figs 2 and 14).

Facies F1 mostly comprises the top part of the outer beach ridge (Figs 4 and 13) and shows onlapping structures and low-angle cross-bedding with seaward inclination. Facies F2 makes up most of the narrow, snaky barrier (Figs 2 and 14). The particle-size distribution peaks in the coarse-sand category; minor peaks at the upper end are caused by single large shells (Fig. 15). Some isolated patches, where the sandstone is cemented (for example, AZ-W2 in Fig. 3) and preserves fenestral structures (Fig. 15), stand out for up to 1 m above the non-cemented barrier (for example, AZ-W3 in Fig. 3 or Fig. 15), indicating post-depositional deflation.

Facies G is only observed in AZ-T2, where it occurs in two patches on top of the sequence (Fig. 13). Facies H occurs as lenses or thin onlapping strata mostly intercalating with Facies F1 in AZ-T2, where it may fill small channel-like structures (Fig. 13). Facies I only occurs inside small channel structures where it overlies Facies H. Facies J1 generally underlies F1. Both facies are similar, whereas J1 shows distinct wavy bedding (Fig. 13).

Age data

Radiocarbon data from sediment cores and surface samples

Radiocarbon dating of bulk carbonate sediment from basal Facies E2, overlying the Dammam limestone, reveals the oldest, Pleistocene ages in cores AZ-W1 (27 475 to 27 180 cal yr BP), AZ-W3 (22 490 to 22 275 cal yr BP), AZ-W4 (39 719 to 38 511 cal yr BP) and AZ-W5 (38 529 to 36 979 cal yr BP). A cerithid shell found in Facies E2 in core AZ-W7 (9.25 m b.s.), however, was dated to 5381 to 4963 cal yr BP, while the

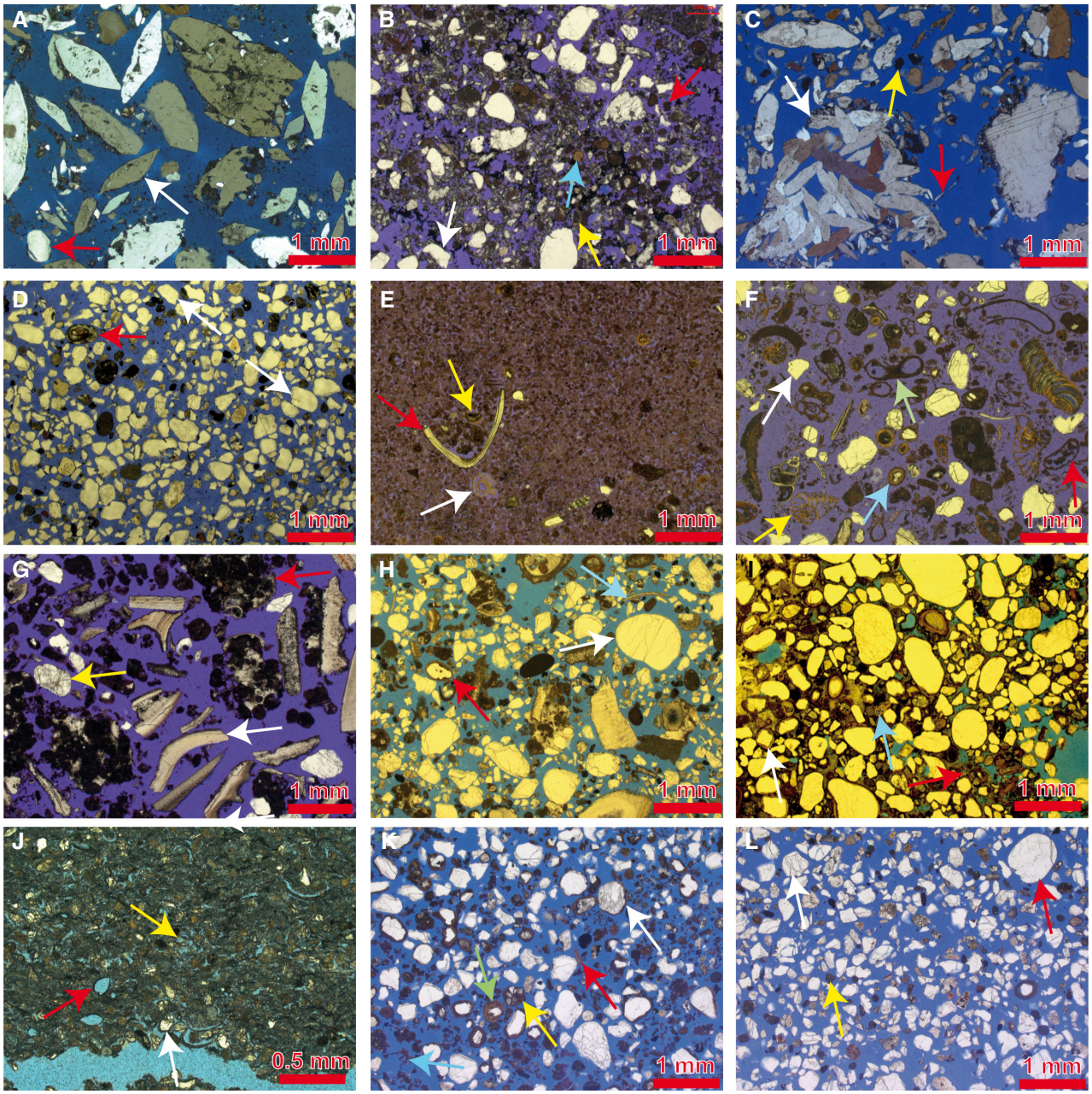

uppermost dating of Facies E1/E2 right below the contact with Facies D1 is 8332 to 8134 cal yr BP (microbial mat in AZ-W4; Figs 3 and S6). Right above the contact, ^{14}C data of Facies E1 and the lowermost part of Facies D1 range between 7917 to 7658 cal yr BP (cerithid shell; AZ-W12) and 6009 to 5702 cal yr BP (bivalve shell fragment; AZ-W5) with an apparent trend towards younger ages inland, where the contact between Facies E1/E2 and Facies D1 rises (Fig. 4).

Facies D1, present in all cores, accumulated over several millennia. Its upper part shows constantly younger ages towards the south reaching from 5551 to 5276 cal yr BP in the north (bivalve shell fragment in AZ-W1; cerithid shells: 5540 to 5235 cal yr BP and 6612 to 6312 cal yr BP), to 3728 to 3397 cal yr BP in the central part of the sabkha (bivalve shell fragment; AZ-W5) and 1869 to 1565 cal yr BP in the southernmost core AZ-W12 (cerithid shell; parallel dating of plant remains: 2355 to 2184 cal yr BP). Facies D1 is overlain by Facies C1 (central part of the sabkha) and C2 (northern and southern ends of the sabkha), respectively, which are dated to 5585 to 5310 cal yr BP in the north (AZ-W3; cerithid shell), 2511 to 2139 cal yr BP in the centre (AZ-W5;

Fig. 6. Thin sections of facies identified in the study area. (A) Facies A (sabkha): lenticular gypsum crystals (white arrow), low amount of rounded quartz grains (red arrow), non-cemented [sample W1/2, 12 to 9 cm below surface (b.s.), ×2.5, crossed polarized light (XPL)]. (B) Facies A (sabkha): wackestone, angular to moderately rounded quartz grains (white arrow) and fine carbonates (red arrow), low amount of skeletal grains (yellow arrow) and ooids (light blue arrow), slightly cemented by gypsum, carbonate and halite matrix (surface crust) (W12/1, 4 to 0 cm b.s., ×2.5, XPL). (C) Facies B (saline lake): almost pure lenticular gypsum, partly aggregated (white arrow), needles (red arrow), very few subangular quartz grains and dark aragonite (yellow arrow) (W5/5, 24 to 21 cm b.s., ×2.5, XPL). (D) Facies C1 (low-energy protected lagoon – quartz-dominated): subangular to subrounded quartz grains (white arrows), fine to medium sand, foraminifera (red arrow), fine skeletal grains [W1/5, 55 to 50 cm b.s., ×2.5, plane polarized light (PPL)]. (E) Facies C2 (low-energy protected lagoon – carbonate-dominated): packstone, peloid-dominated, with foraminifera (white arrow), shell fragments (red arrow) and ostracods (yellow arrow) (W11/6, 90 to 80 cm b.s., ×2.5, PPL). (F) Facies D1 (mid-energy open lagoon): packstone, poorly sorted, subangular quartz grains (white arrow) and high concentration of skeletal material [mostly ostracods (red arrow), foraminifera (yellow arrow), gastropods, bivalves], minor ooids (light blue arrow), abundant serpulids (light green arrow), often showing straight attachment surfaces, indicate growth on seagrass leaves (W11/10, 250 to 240 cm b.s., ×2.5, PPL). (G) Facies D1 (mid-energy open lagoon): packstone–wackestone, non-cemented, large shell fragments (white arrow), smaller skeletal fragments aggregated with peloids (red arrow), minor amount of moderately sorted, rounded quartz grains (yellow arrow) (W10/16, 333 to 323 cm b.s., ×2.5, PPL). (H) Facies D2 (high-energy open lagoon): quartz-rich grainstone, poorly sorted, moderately to well-rounded (white arrow), coated quartz grains (pseudo-ooids) (red arrow), foraminifera, ostracods, serpulids, mollusc fragments (light blue arrow) (W7/23, 665 to 660 cm b.s., ×2.5, PPL). (I) Facies D2 (high-energy open lagoon): carbonate-rich sandstone, moderately to well-rounded, coated quartz grains (superficial ooids) (white arrow), cemented by fibrous aragonite (hardground) (red arrow), very low amount of skeletal material (light blue arrow) (W7/24, 677 cm b.s., ×2.5, PPL). (J) Facies D3 (low-energy, deeper subtidal): packstone, fine-grained peloids and skeletal grains, subangular quartz grains, many of them coated (pseudo-ooids) (white arrow), ostracods (red arrow) and foraminifera (yellow arrow), mm-bedded (W6/57, 1465 to 1460 cm b.s., ×5.0, PPL). (K) Facies E1 (reworked dune – transgressive): sand, frosted and coated quartz grains (pseudo-ooids) (white arrow), minor amounts of peloids and skeletal grains (red arrow), some foraminifera (yellow arrow), ostracods (light blue arrow) and ooids (light green arrow) (W5/20, 440 to 430 cm b.s., ×2.5, PPL). (L) Facies E2 (aeolian dune): sand, subangular (white arrow) to (sub-)rounded (red arrow), frosted quartz grains, moderately to well-sorted, very minor amounts of dark carbonates (yellow arrow), non-cemented, no skeletal components (W5/29, 780 to 748 cm b.s., ×2.5, PPL).

articulated bivalve shell), and 1794 to 1479 cal yr BP in the south (AZ-W12; cerithid shell). A comparison between AZ-W5 and AZ-W9, where the upper part of Facies C1 is dated to 3711 to 3390 cal yr BP (cerithid shell), shows that its accumulation stopped significantly earlier at the landward margin of the sabkha. Facies C is in most of the cores overlain by Facies B and A, for which no ages could be obtained, apart from surface dates shown in Fig. 2.

The snaky barrier (Facies F2) shows a radiocarbon date of 5886 to 5611 cal yr BP (AZ-W3; gastropod shell). The seaward barrier (mainly Facies F1) shows a broad distribution of ^{14}C data: In the wide, central section, ages of 6443 to 6191 cal yr BP, 5826 to 5516 cal yr BP (AZ-W6; cerithid shells) and 5238 to 4856 cal yr BP (AZ-W7; cerithid shell) were obtained from the central and landward part of the barrier; some of them are not in stratigraphic order. The ages from the seaward part of the barrier obtained in the north are younger, ranging from 3609 to 3316 cal yr BP at the landward edge of AZ-T2 to 1217 to 938 cal yr BP at its seaward end. A cerithid surface from cemented surface beachrock at the narrow palaeo-spit inland of the main barrier in the central part of the sabkha provides an age of 3755 to 3417 cal yr BP (AZ-Spit 1; Fig. 2), whereas a cerithid shell from the active beach in the south gives a modern age. In general, there is a stark contrast between surface data from the very northern, sandy landward margin of the sabkha (5534 to 5209 cal yr BP and 5440 to 5061 cal yr BP at AZ-OSL-7; articulated *Hiatula mirbahensis* and cerithid shells) and those from the southern counterpart ranging from 3387 to 3065 cal yr BP (AZ-6-12; cerithid shell) to 1036 to 752 cal yr BP (AZ-3-12; cerithid shell).

The age distributions from the vibracores, including adjacent surface data (Fig. 2), show no inconsistencies. Where different material is dated from the same stratigraphic depth, the 2σ age spans either overlap (AZ-W1), show moderate or, as in one case only, extreme discrepancy (AZ-W12). Radiocarbon data from the deeper wells AZ-W6 and AZ-W7, however, almost entirely fall into the range of 6000 to 5000 years ago and show numerous inconsistencies (Fig. 4).

Optically stimulated luminescence (OSL) ages

A comparably large scatter of equivalent-dose (D_e) distributions is observed in all OSL samples. However, while AZ-T1 and AZ-W7 show normally

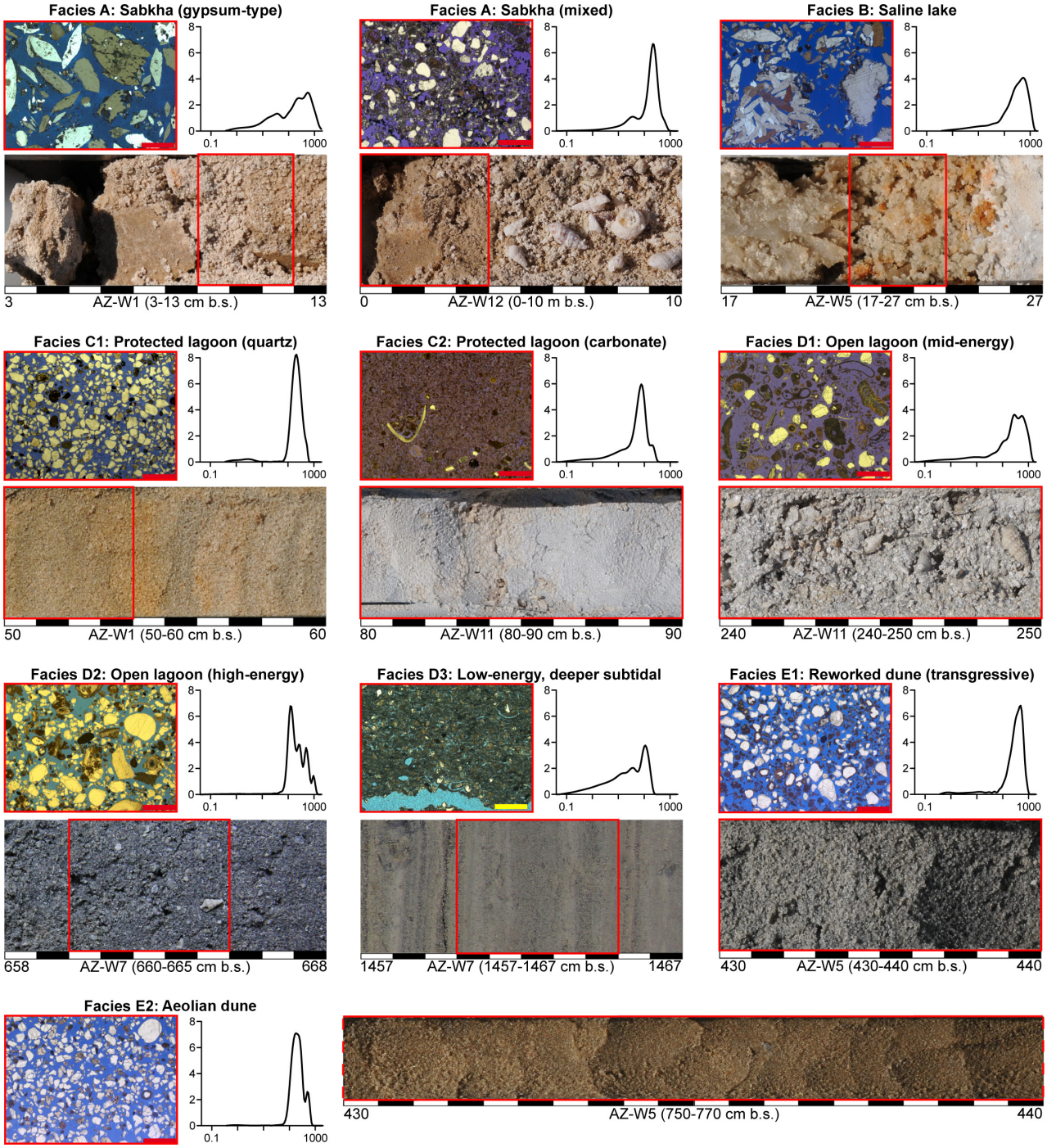

Fig. 7. Thin sections, core sections and grain-size distribution of the sabkha facies types. Details on thin sections can be found in Fig. 6. The red frame on the core sections indicates where samples for thin sections and grain-size analysis were taken. Grain-size diagrams: x axis = grain size (μm), y axis = amount of grains in specific class (vol. %). Red scale bar = 1 mm, yellow scale bar = 0.5 mm.

distributed D_e with moderate over-dispersion values of 17 to 63%, the AZ-T2 samples are characterized by over-dispersion values of 84 to 100% and right-skewed dose distributions (Fig. S1).

The OSL age estimate from Facies E2 at the base of AZ-W7 (Figs 4 and S5) gives a latest Pleistocene, pre-transgressive age of 12060 ± 910 years. Samples of the narrow, snaky barrier, for which the

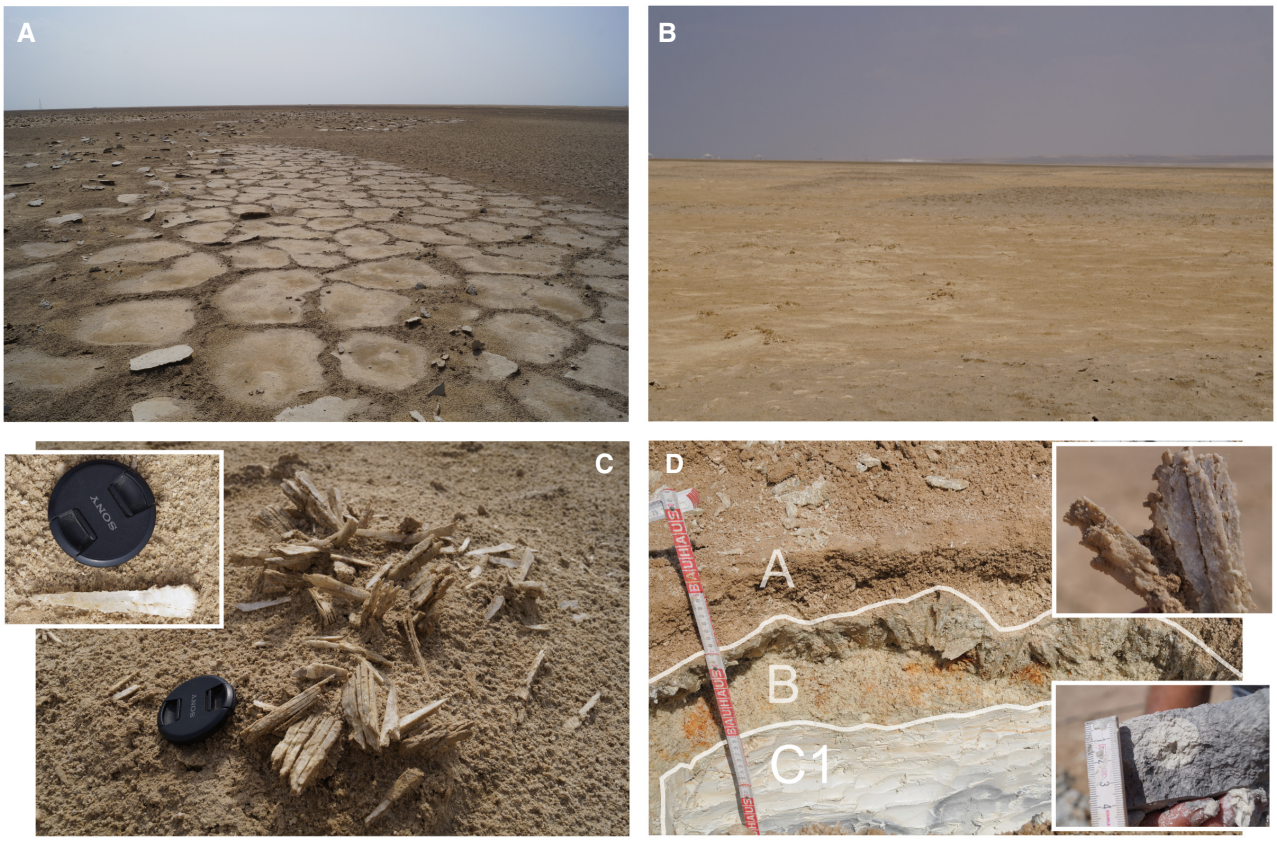

Fig. 8. Surface patterns of evaporites. (A) Ephemeral halite-dominated crust in the southern central part of the sabkha near AZ-W10 forming a typical polygonal pattern. The transition to the prevailing buckled gypsum crust and tepee structures in the upper right is sharp. The diameter of the polygons is mostly between 50 cm and 80 cm. (B) Circular mounds of buckled gypsum crust (dark brown) in the centre near AZ-W5 elevated by large prismatic gypsum growing right below the surface. The mound in the central part of the picture has a diameter of *ca* 15 m. (C) In some of these cases, prismatic gypsum breaks the surface, dehydrates and transforms into bassanite/anhydrite, as exemplified in the insert, where the transformed whitish part (bassanite/anhydrite) experienced subaerial exposure. (D) The central part of the sabkha at AZ-W5 shows the typical sequence of white carbonate mud with traces of bioturbation (see lower insert) (Facies C1), pure gypsum mush, large swallow-tail gypsum (see upper insert) (Facies B), overlain by a mixture of prismatic and lenticular gypsum crystals, quartz sand and halite, protected by a thin buckled crust (Facies A).

central age model (CAM; Galbraith *et al.*, 1999) was chosen, are dated to 7682 ± 884 years and 5414 ± 467 years (AZ-T1). At AZ-T2, ages of 1244 ± 118 years and 918 ± 229 years were obtained using the minimum age model (MAM; Galbraith *et al.*, 1999) for the landward and seaward ends of the trench, respectively.

DISCUSSION

Resolving the facies architecture of the Al-Kharayej sabkha

Facies E2: Pre-transgressive dunes

The moderately to well-rounded quartz grains of Facies E2 underlie the transgressive wedge of the sabkha and represent the aeolian dunes of the dry, late Pleistocene Gulf of Salwa. Its characteristic unimodal grain-size distribution corresponds to modern aeolian sands of barchan dunes and surface depressions found in Qatar today (Embabi & Ashour, 1993; Engel *et al.*, 2018, 2020) and is directly related to the drowned barchan dunes, which have been identified inside the Gulf of Salwa (Kassler, 1973; Al-Hinai *et al.*, 1987).

Facies E1: Reworked dune (transgression facies)

The rounded quartz grains with minor carbonate coating and minor amounts of carbonate of Facies E1 (Fig. S6A) represent dune sand

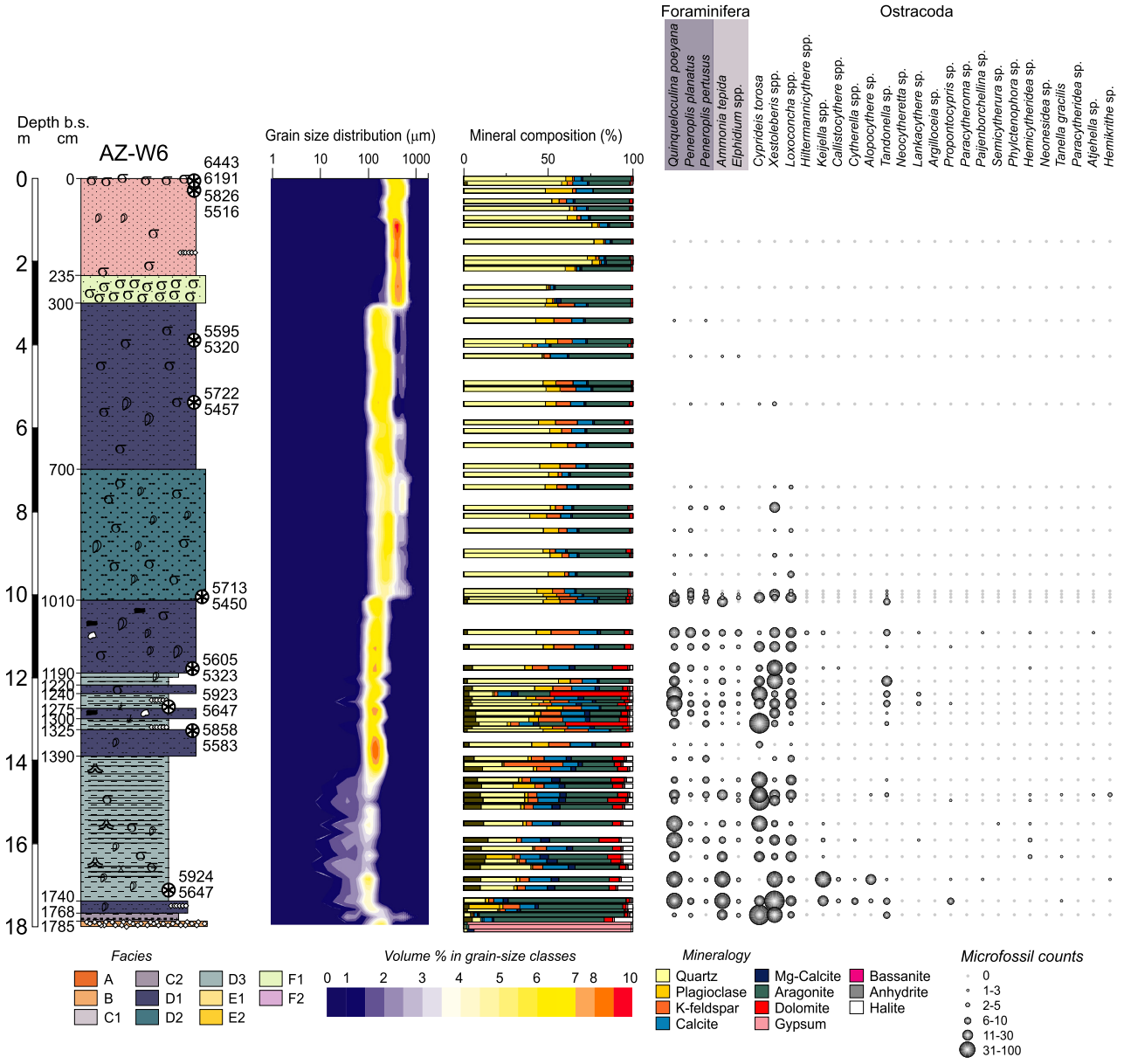

Fig. 9. Deep well AZ-W6 (location in Fig. 2) on top of the outer barrier, with core log as well as data on grain-size distribution, mineralogy and microfossil content. A legend for the core log is shown in Figs 3 and 5.

overprinted by marine reworking during the rapid early to mid-Holocene transgression. E1 occurs in the form of a thin transition layer between the predominantly late Pleistocene dunes (E2) and the coarse-grained, mid-energy open lagoon (D1) throughout the sabkha.

Facies D1: Mid-energy open lagoon to open coast

The medium to coarse-grained skeletal–peloidal packstone, poorly sorted and with minor occurrences of coated quartz grains, indicates a higher-energy environment, i.e. a subtidal, open-lagoon environment. Its thickness of up to several metres in the entire sabkha corresponds to rapid accumulation during the RSL highstand in the southern Arabian Gulf around 6000 to 4500 years ago (Lokier *et al.*, 2015; Strohmenger & Jameson, 2018; Parker *et al.*, 2020; Rivers *et al.*, 2020). In contrast to C2, Facies D1 lacks shallow, protected-lagoon ostracods of *Cyprideis torosa* and *Hemicytheridea*, but shows a higher diversity, which

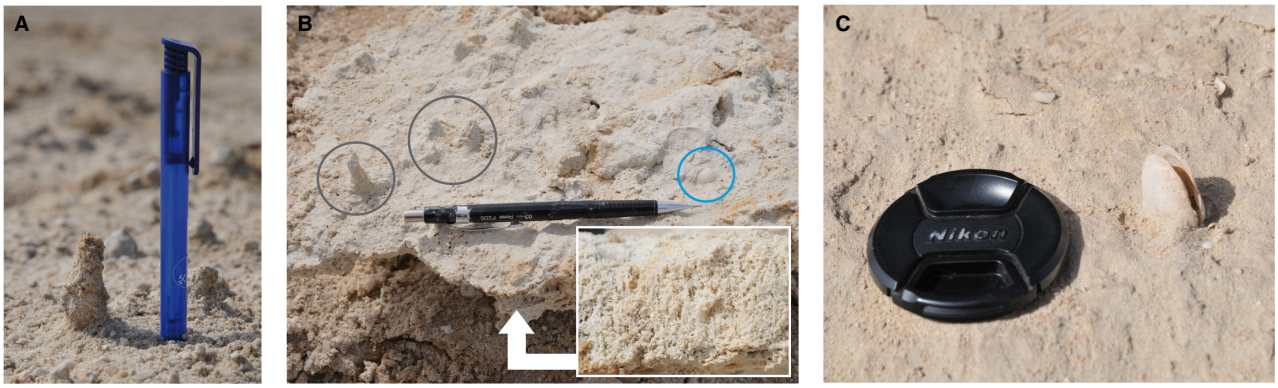

Fig. 10. (A) Vertical burrows preserved in Facies C1 near AZ-W4 indicate prevailing deflation of the surrounding material. (B) Where not overlain by Facies A (supratidal sabkha) or B (saline lake, salina), Facies C1 (low-energy protected lagoon) may form a carbonate crust which close to AZ-W4 also suffers from deflation and corrasion indicated by the exposed burrows (grey circle) and small exposed shells (blue circle). Pens for scale are *ca* 14 cm long. (C) Articulated bivalves of *Hiatula mirbahensis* were even found in living position and exposed at the surface by deflation in the north near AZ-W1. Lens cap is 5.5 cm in diameter.

may be attributed to a decrease in terrigenous input in the deepening lagoon (Mostafawi, 2003). It is also rich in serpulids, often showing straight attachment surfaces, indicating growth on seagrass leaves (Fig. 6F). The abundant ostracod taxa of *Loxoconcha* spp. and *Xestoleberis* spp. have also been found to be dominant elsewhere in moderately restricted parts of the Gulf of Salwa (Hughes Clarke & Keij, 1973).

Facies D2: High-energy open lagoon to open coast

The coarse-grained sand with varying amounts of skeletal debris representing D2 is only found in deep well AZ-W7 on the outer barrier. It represents the highest-energy facies of the study area. It is very similar to Facies D1, but slightly coarser and contains a higher number of coated quartz grains, which are typical for higher-energy, outer lagoon environments of the Gulf of Salwa (Rivers *et al.*, 2019b).

Facies D3: Deeper subtidal

The laminated fine-grained peloid–skeletal packstone is also only found relatively deep in AZ-W7, where it alternates with Facies D1. It likely corresponds with the rapid transgression until 7000 to 6000 years ago leading to quick flooding and water depths of several metres. Whether the alternation of D1 (coarse-grained) and D3 (fine-grained) in AZ-W7 is the result of rapid vertical fluctuations in relative sea-level, event-type, storm-wave deposition, or lateral coastal changes remains open.

Facies C2: Low-energy, carbonate-dominated lagoon

Facies C2 represents a low-energy, carbonate-dominated lagoon. It is characterized by a high amount of autochthonous aragonite mud and low input of aeolian sand. In AZ-W10, the foraminiferal assemblage of the upper part of C2 is dominated by *Ammonia tepida* and *Elphidium* spp. *Ammonia* and *Elphidium* represent the only foraminiferal taxa in the very shallow (<1 m) parts of a protected, siliciclastic embayment along the Saudi Gulf coast, explained by the resistance of their tests against mechanical abrasion (cf. Arslan *et al.*, 2016). *Ammonia tepida* is also the most common species in the mud-dominated tidal flats of Kuwait, northern Gulf (Al-Abdul-Razzaq *et al.*, 1983). In the lower part of C2 in AZ-W10, *Quinqueloculina* spp. becomes abundant – besides *Peneroplis planatus* and *P. pertusus* – which is very common in the intertidal to deeper subtidal environments of the southern Gulf (Ahmed, 1991). The ostracod *Hemicytheridea*, also associated with very shallow, restricted conditions of inner embayments (Al-Abdul-Razzaq *et al.*, 1983), occurs only in C2 in significant numbers. *C. torosa* is only found in the upper part of C2, where it supports the interpretation of a shallow, sheltered and hypersaline lagoon environment according to its high abundance in similarly challenging environments of Abu Dhabi (Bate, 1971; Stewart *et al.*, 2011).

The high amount of aragonite in C2 (Fig. 11) derives from evaporation-driven salinity increase,

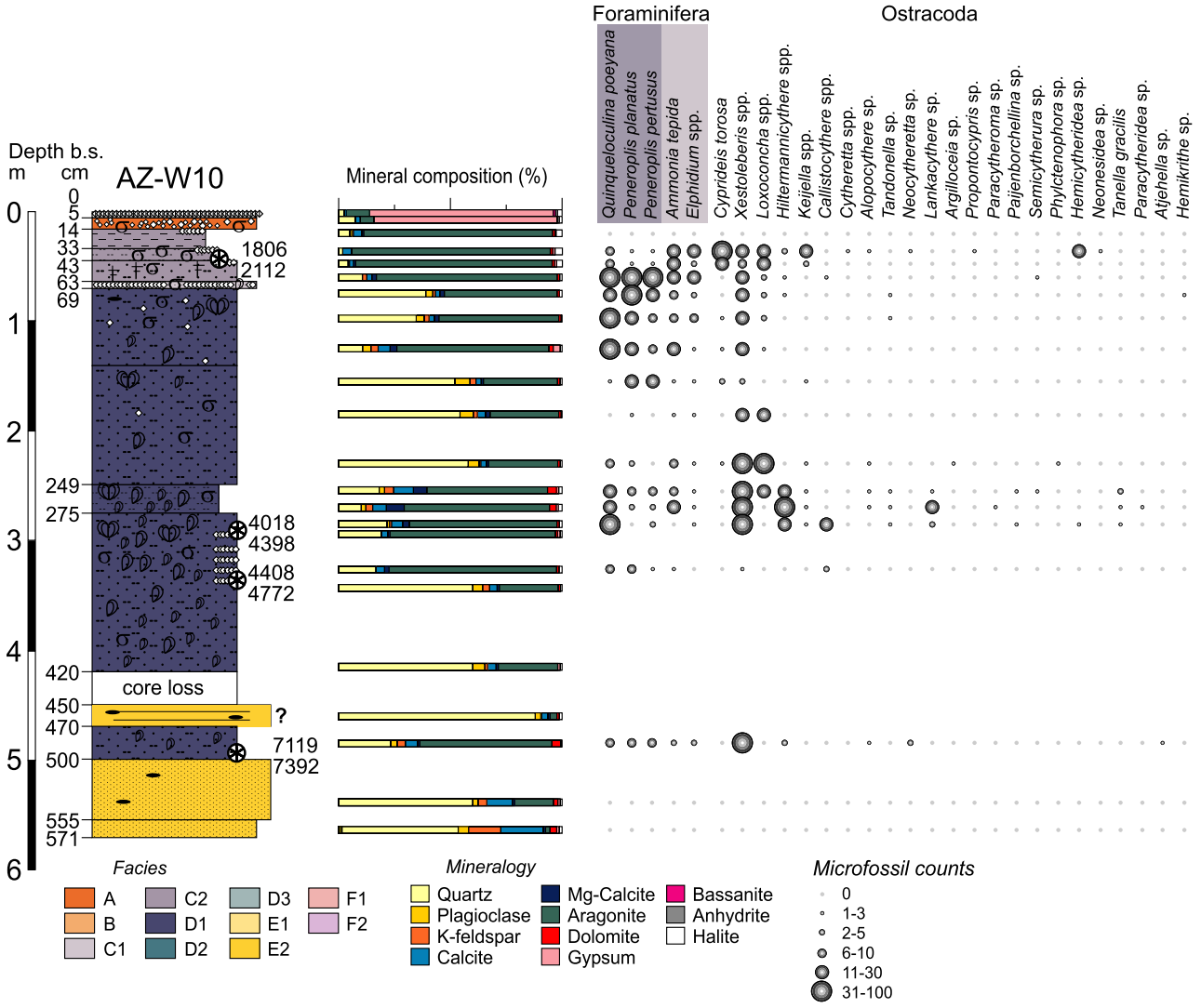

Fig. 11. Sediment core AZ-W10 (Fig. 2) with core log and data on mineralogy and foraminifera and ostracod content. Colour codes for mineral composition and a legend for the core log are shown in Fig. 3.

which in marginal-lagoon settings of Qatar may add up to 90 psu, and diagenetic aragonite precipitation in the water column. Further salinity increases following marine regression, and gradual shallowing and silting up of the lagoon under evaporation pressure then leads to gypsum and halite precipitation towards the top of the sediment column (Facies B and A) (Rivers *et al.*, 2019b). With its hardground at around the groundwater level in AZ-W10 (Fig. 11), Facies C2 corresponds to the bioclastic or peloid–skeletal packstone of the lowermost intertidal to shallow subtidal lagoon environment identified by Strohmenger *et al.* (2011) near Al-Qanatir (Al-Rufayq) Island and by Strohmenger *et al.* (2010) inside the Mussafah Channel (both Abu Dhabi). It also corresponds to the soft-pelleted, skeletal lime muds of the restricted, shallow lagoons of Sabkha Faishakh and Sabkha Hussain, north-western Qatar (Taylor & Illing, 1969; Illing & Taylor, 1993).

The separation between open-lagoon (D1) and protected low-energy lagoon (C2) facies is clearly demonstrated by the PCA of proxy data of AZ-W10 (Fig. S7). Principal component (PC) 1 explains >40% of the distribution. Based on the negative values of aragonite, which is mostly present in the low-energy lime muds (e.g. Illing & Taylor, 1993), and positive values of quartz, derived from the reworking of dunes in higher-

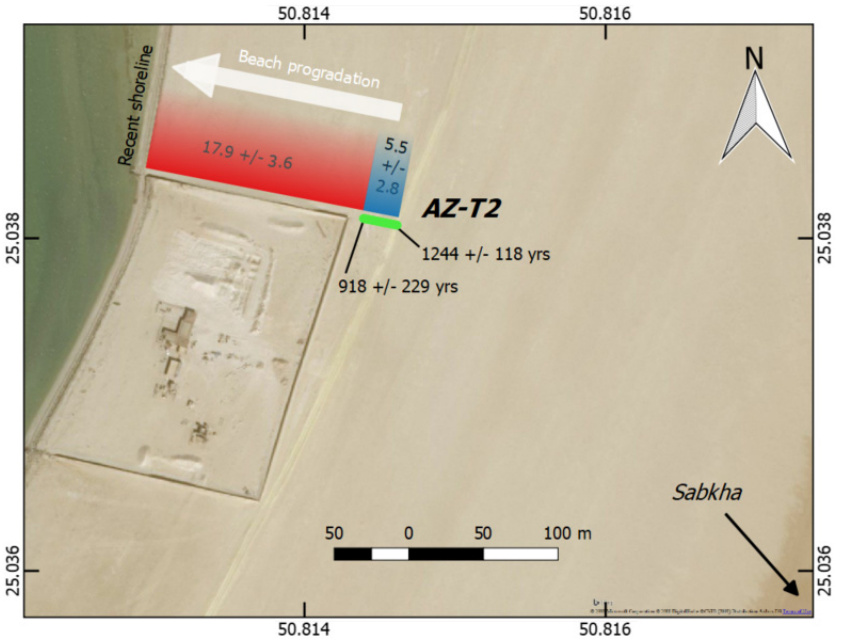

Fig. 12. Location of transect AZ-T2 (green line) at the northern seaward part of the outer barrier, which delineates the sabkha. The location of the map is shown in Fig. 2. Annual rates of barrier progradation (in cm yr^{-1}) are inferred from optically stimulated luminescence (OSL) data from AZ-T2 (Tables S2 and S3; Fig. 13) (satellite image from 13 October 2013; copyright DigitalGlobe, accessed through Bing Maps).

energy environments, PC 1 is interpreted to positively correlate with hydraulic energy, i.e. low values representing protected-lagoon conditions (C2) and high values representing higher-energy open-lagoon conditions (D1). PC 2 may positively correlate with water depth.

Facies C1: Low-energy, sand-dominated lagoon

Facies C1 represents a low-energy, sand-dominated lagoon, similar to C2, but with a significantly higher input of quartz sand. Macrobenthic and microbenthic remains indicate a shallow and protected lagoon, still permanently connected to the Gulf of Salwa. Parts of this lagoon may have been intertidal, as *Hiatula mirbahensis* bivalves, found in living position, endure temporary exposure and usually populate such soft, fine-sandy to muddy, protected habitats along the Emirates coast (Morris & Morris, 1993; Feulner & Hornby, 2006). Likewise, *Peneroplis planatus* is abundant in the intertidal zone of the low-inclination coastlines along the southern Arabian Gulf (Al-Abdul-Razzaq *et al.*, 1983; Ahmed, 1991; Al-Kathany *et al.*, 2015). In Qatari waters, the genus *Peneroplis* was found in the shallowest environments (Al-Hitmi, 2000). Ostracods of the genus *Xestoleberis*, i.e. *X. rhomboidea* and *X. rotunda*, which dominate Facies C1, are also associated with soft-bottom intertidal zones of protected bays along the southern and western Gulf. They are competitive in high salinities (42 to 72.45‰) and a wide range of water temperatures (21 to 35°C) (Al-Abdul-Razzaq *et al.*, 1982; Mostafawi, 2003). The second prominent genus, *Loxoconcha* spp., could not be determined to species level. Four species of *Loxoconcha* have been identified along the coast of the southern Arabian Gulf. They are predominantly distributed on the nearshore shelf, but also in tidal channels and protected lagoons (Bate & Gurney, 1981).

In the north, C1 formed during the mid-Holocene (AZ-W1; Fig. 3). Quartz sand dominates and indicates long-distance aeolian input by the Shamal at a time when upwind dune fields in the north-western peninsula still existed (cf. Engel *et al.*, 2018). The occurrence of similar Facies C2 grainstone in the south (AZ-W12; Fig. 3) at a later stage during the late Holocene, when upwind sand sources had ceased (cf. Engel *et al.*, 2018), is dominated by aragonite, testifying to only local aeolian input from the seaward barrier which, to a large part, consists of skeletal grains.

The protrusion of articulated *H. mirbahensis* and exposure of vertical burrows (Fig. 10A and B) in the northern part around AZ-W4 (Figs 2 and 3) indicate deflation driven by a gradual lowering of the capillary fringe to produce a Stokes surface (Fryberger *et al.*, 1988), which in

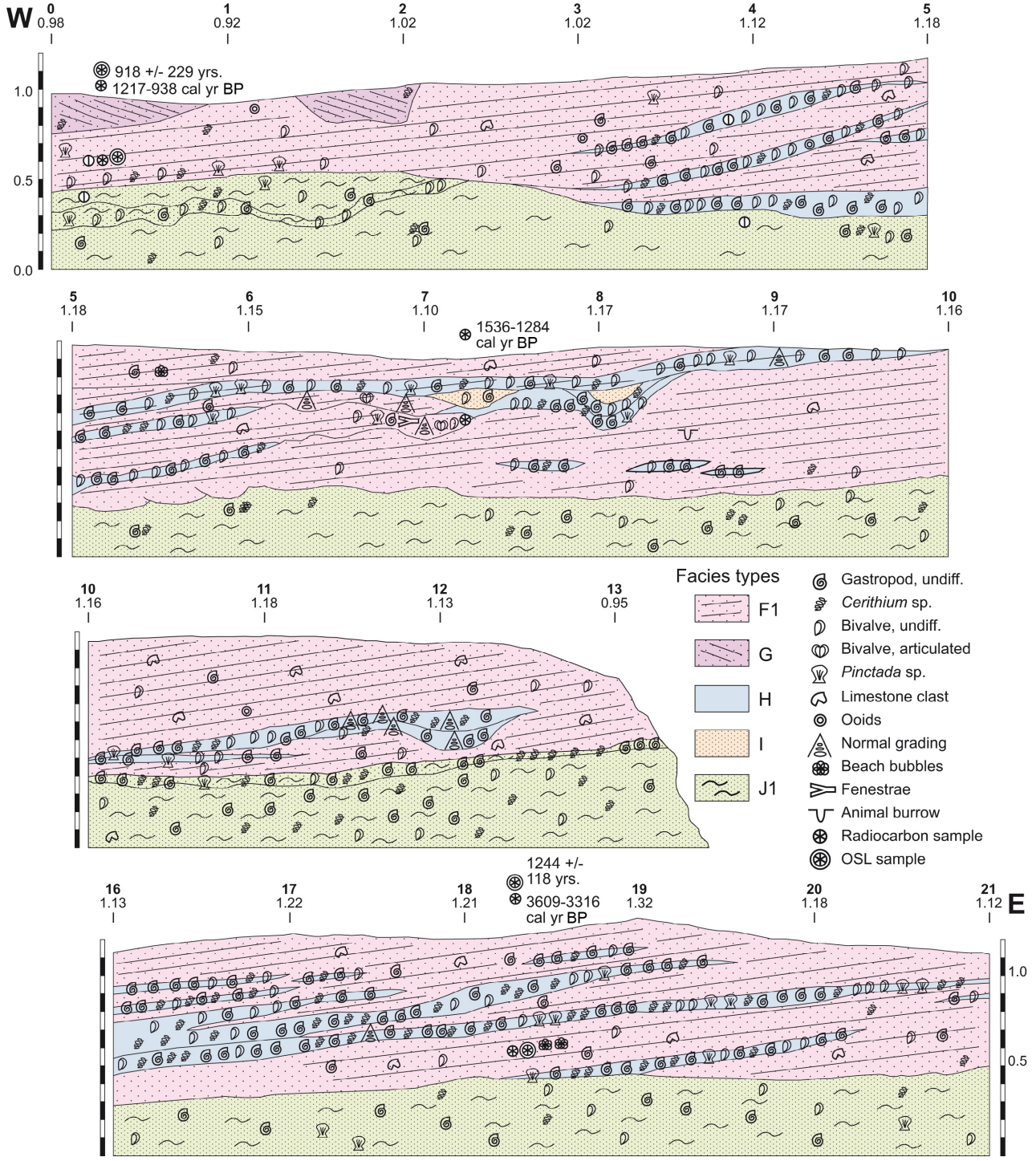

Fig. 13. Trench AZ-T2 (for location see Figs 2 and 12) showing the facies architecture of the northernmost seaward barrier. It is separated into four sections and has a gap between *ca* 13.5 m and 16 m from its western end (numbers in bold on top of the profile sections refer to distance in metres from the western end of the trench; those in regular font indicate the thickness of the profile in metres).

Qatari sabkhas lies mostly around 0.5 m above the groundwater table (Whitaker *et al.*, 2014). In the Asaila Basin, central-eastern Qatar, deflation is also dominant and controlled in a similar way by a lowering groundwater level and Stokes surface after the mid-Holocene RSL highstand. Ground

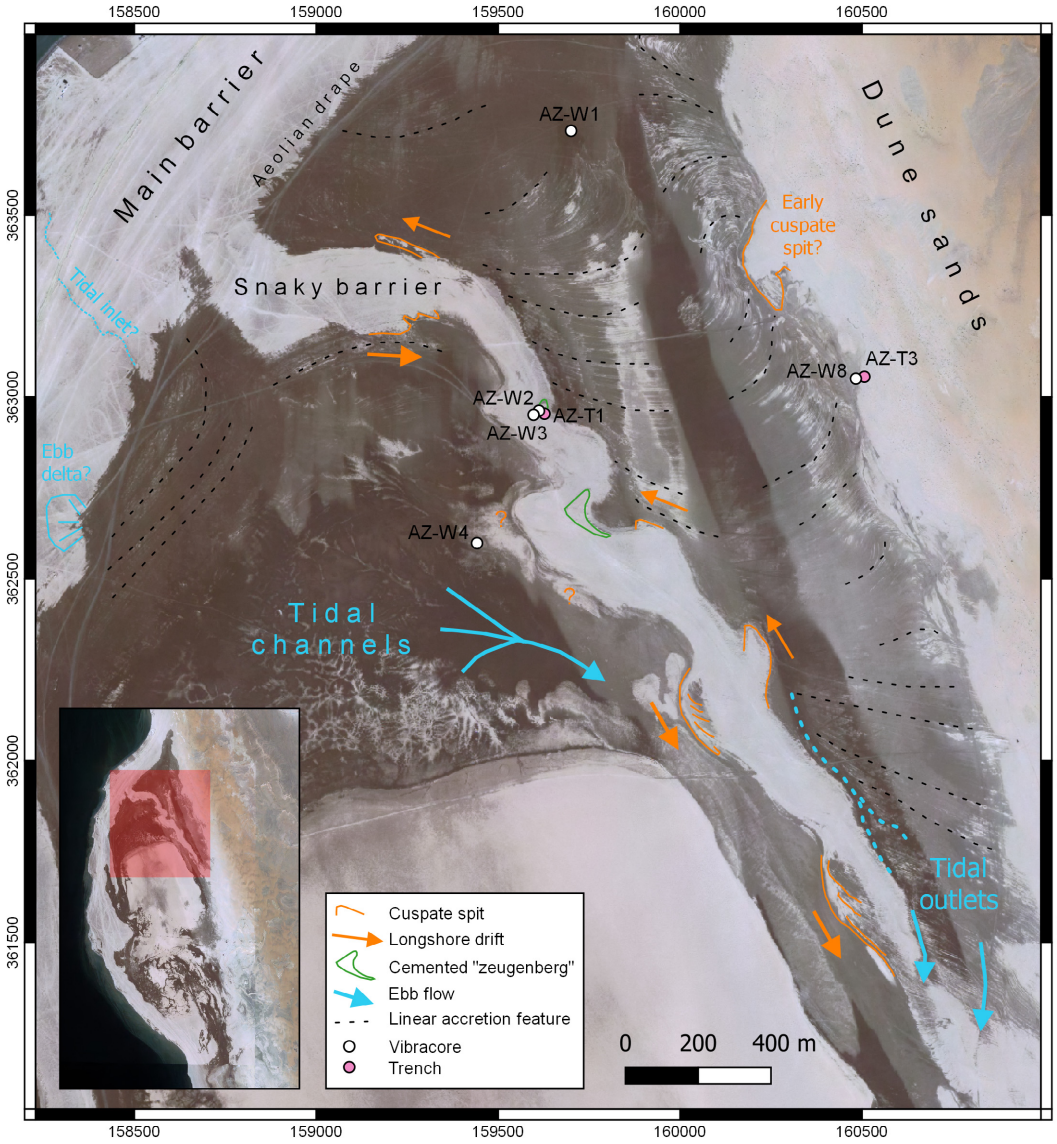

Fig. 14. Geomorphic features of the snaky spit and the sabkha floor (based on WorldView 2 satellite image from 2011).

surface lowering has been estimated to a minimum of 1.5 m, inferred from the elevation of remnant yardang-type mounds (Engel *et al.*, 2020).

Facies B: Saline lake/lagoon (salina)

Facies B only occurs in the very central part of the sabkha (AZ-W5), where, in combination with the overlying supratidal sabkha deposits, it forms a regressive evaporite sequence. The prismatic gypsum mush (selenite) embedded in a soft, grey mud followed by a layer of large displacive and replacive twinned gypsum minerals of >10 cm length, indicate subaqueous formation from a highly concentrated brine in the final, shallow stages of the salina body (Warren, 1996; Strohmenger & Jameson, 2018). Extremely high surface temperatures during summer dehydrate and transform exposed parts of prismatic gypsum crystals (swallow tails) to bassanite/anhydrite (exposed, whitish parts in Fig. 8C).

Facies A: Recent supratidal sabkha

Gypsum-encrusted and halite-encrusted quartz grains, as well as lenticular and prismatic gypsum crystals in Facies A, combined with a buckled crust, are typical for active supratidal

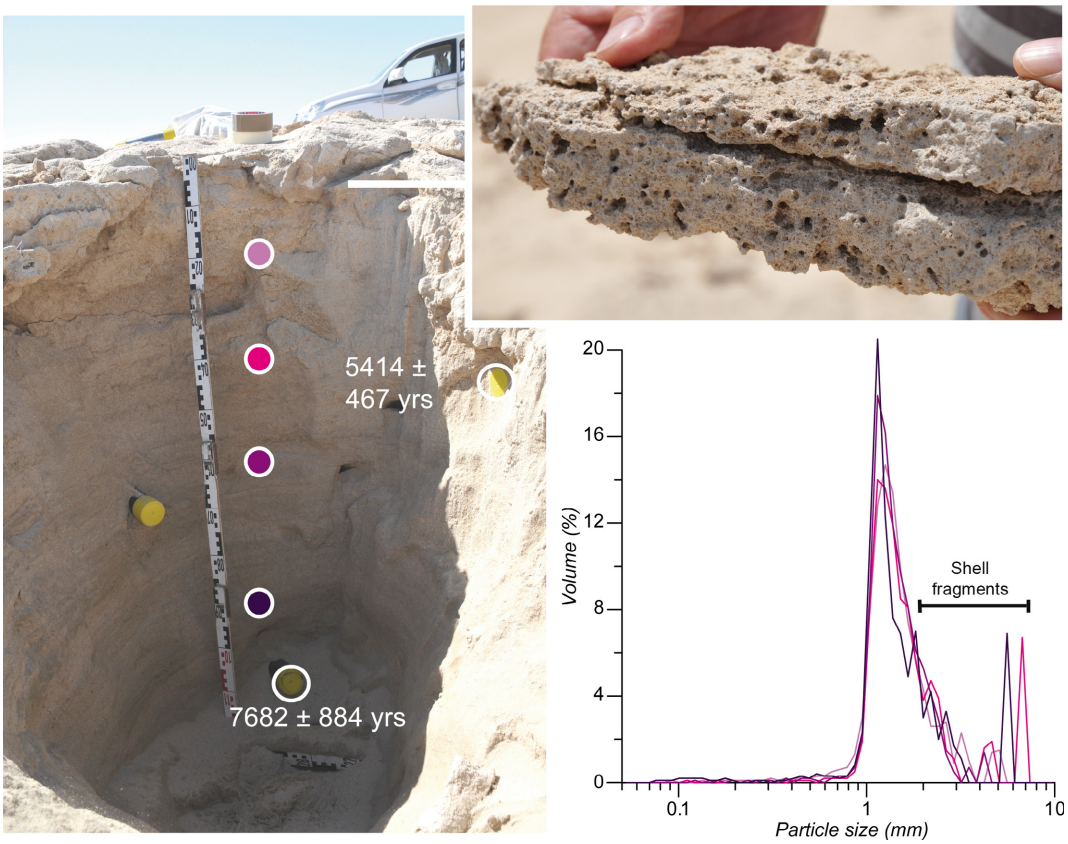

Fig. 15. Trench AZ-T1 on top of the narrow, snaky barrier crossing the northern sabkha (Figs 2 and 14). Sampling depths for grain-size distribution (five samples: lower right diagram) and optically stimulated luminescence (OSL) dating (Tables S2 and S3) are shown, along with a detail photograph of cemented sandstone with fenestral structures (upper right). From the three OSL samples (yellow tubes), only two were eventually dated.

sabkha environments (e.g. Al-Yousef, 2003; Strohmenger *et al.*, 2011; Strohmenger & Jameson, 2015). In some places, clear polygonal structures are indicative of supratidal conditions (Billeaud *et al.*, 2014). In Facies A, a small percentage of gypsum is replaced by bassanite and anhydrite through dissolution and reprecipitation (Gunatilaka *et al.*, 1985; Warren *et al.*, 1985; Alsharhan & Kendall, 2003; Strohmenger *et al.*, 2011), mostly in the capillary zone above the palaeo-groundwater table as thermalites (Wood *et al.*, 2005; Strohmenger *et al.*, 2010). Occasional cerithid shells and small, indeterminable bivalve shell fragments are likely introduced by strong Shamal winds from the seaward barrier, because muddy intertidal feeding grounds with microbial mats and algae cover required by the surface-grazing *Cerithium* sp. (cf. Stewart *et al.*, 2011) are currently absent. Similar modern sabkha environments have been described elsewhere in Qatar, such as in Al Dakhirah (Billeaud *et al.*, 2014) or Sawda Nathil (Strohmenger & Jameson, 2018).

Thus, the parasequence described here, starting with pre-transgressive dunes (E2), overlain by reworked dunes (E1), open lagoon (D1), protected lagoon (C1/C2), salina and sabkha deposits (Fig. 3), is quite similar to the classical sabkha sequence often found along the southern coast of the Arabian Gulf (e.g. Alsharhan & Kendall, 2003; Evans, 2011; Strohmenger *et al.*, 2011).

Resolving the barrier architecture

Facies J1: Mid-energy upper shoreface

The skeletal–peloid grainstone of Facies J1 underlies the foreshore and represents the shallow subtidal upper shoreface (Fig. 13). The coexistence of planar and wavy or trough cross-

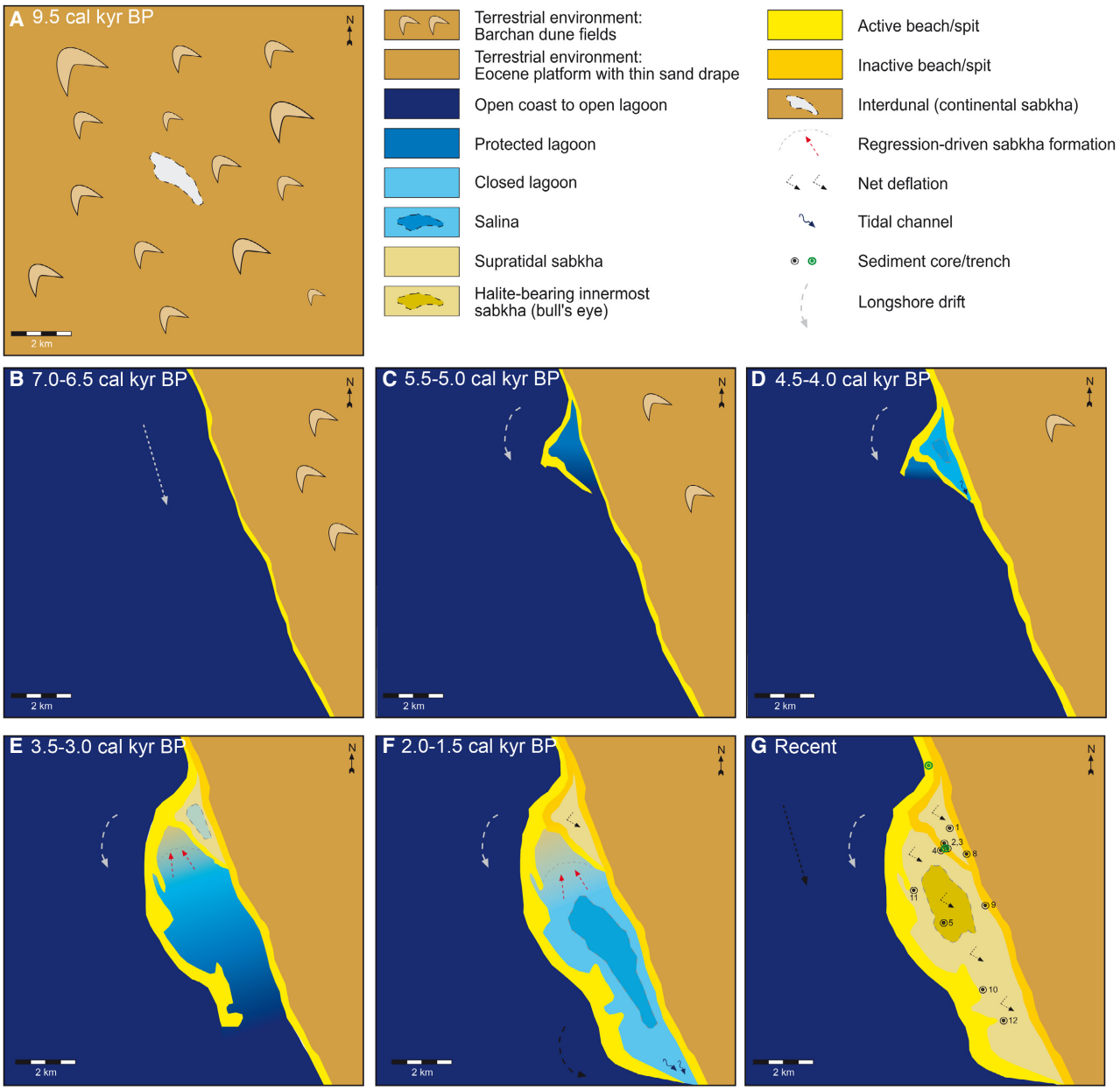

Fig. 16. (A) to (G) Scenarios of beach, lagoon and sabkha formation at Al-Kharayej during the Holocene based on the age data and facies model established in this study. For further information, refer to text. Numbers in (G) indicate the location of the ten vibracores. The green dots indicate the location of the trenches.

beds is characteristic for depositional environments right below mean low water (e.g. Reinson, 1979; Dashtgard *et al.*, 2012).

Facies F1: Outer beach barrier, mid to high-energy foreshore environment

The peloid–skeletal grainstone of Facies F1 with very low-angle seaward inclination makes up the upper, subaerial part of the barrier separating the sabkha from the Gulf of Salwa. The cemented sections with fenestral structures (keystone vugs) indicate formation in the swash zone of the foreshore and later preservation as beachrock. It largely corresponds with the linear ridge of 'type 1 deposit' identified as the mid-Holocene beach associated with landward shallow-lagoon deposits at Al-Ruwais, northern Qatar (Rivers *et al.*, 2020). Mauz *et al.* (2015, p. 7) link "low angle seaward-dipping tabular cross-bedding and

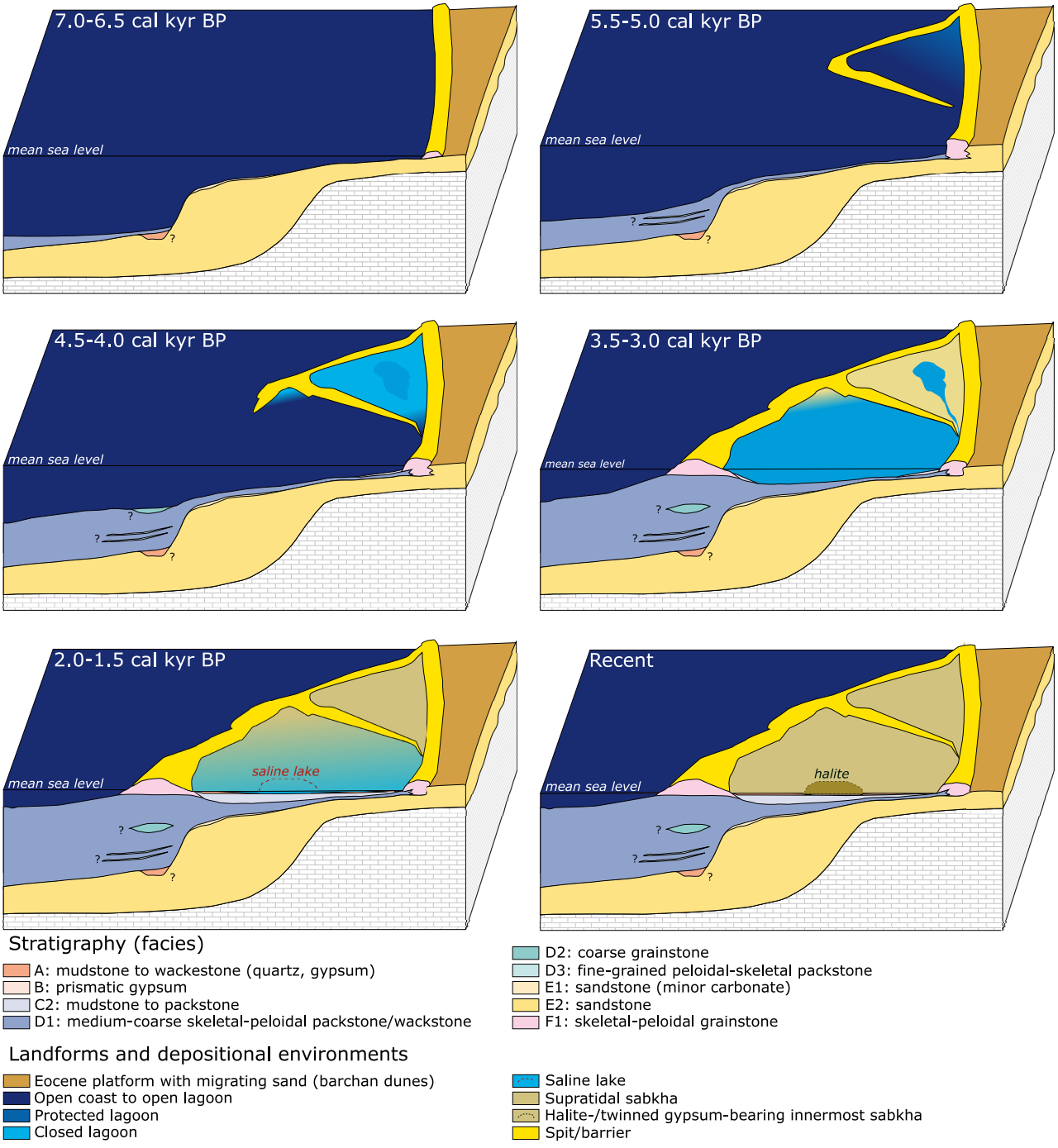

Fig. 17. Scenarios of coastal regression and sabkha formation at Al-Khareyej, combining depositional history and associated coastal landform changes.

keystone vugs" in beachrock with formation from the mean tidal level to mean high-water level.

Facies H: High-energy foreshore

The foreshore of the outer barrier shows several onlap structures of very coarse skeletal–peloid grainstone with massive shells (Fig. 13), indicating higher-energy deposition. Interbedded with F1, they form a progradational, seaward dipping foreshore architecture with several bounding surfaces (e.g. Neal *et al.*, 2002). The distribution of larger mollusc shells in pockets can also be observed in the modern upper foreshore environment.

Facies G: Backshore
In contrast to the dominant occurrence of Facies F1, small sections of the uppermost part of AZ-T2 show landward inclination. These are interpreted as supratidal backshore deposits, mostly resulting from small-scale storm overwash (cf. Davis, 1978; Schwartz, 1982). Thus, the barrier architecture as exposed in AZ-T2 corresponds to the regressive (prograding) barrier parasequence as, for instance, summarized in Reinson (1979).

Facies I: Aeolian deposition in swales
The quartz-dominated Facies I is only found in small backshore depressions. The moderately to well-sorted medium to coarse sand with only few shell components indicates aeolian deposition in the backshore, whereas the absence of vegetation on the barrier prevents proper foredune formation.

Facies F2: Protected beach/spit (snaky barrier)
Sand grains of F2 along the snaky barrier are moderately to well-rounded and show a unimodal distribution, similar to E2. However, the deposit is significantly coarser (peaking in the coarse-sand category) than the aeolian facies. Beachrock cementation, again showing fenestral structures (Fig. 15), support the interpretation of a foreshore environment, but exposed to lower energy compared to F1.

Chronostratigraphy

All calibrated ^{14}C ages represent maximum ages, because *post-mortem* relocation of the dated objects can never be entirely excluded, apart from articulated shells in living position (i.e. *H. mirbahensis*) and the thin microbial mat in AZ-W4. However, the majority of ^{14}C data from the vibracores (AZ-W1 to AZ-W5; AZ-W8 to AZ-W12) in combination with surface samples show no inconsistencies. They are in accordance with the regional RSL history, and can be used with confidence for reconstructing sabkha formation in space and time. Nevertheless, multiple datings from the same depth in the upper part of Facies D1 in AZ-W12 (Fig. 3) show that individual ^{14}C data could be overestimating the age of sedimentation by up to several hundreds of years.

The ^{14}C data from Facies E2 ranging from 22 000 to 40 000 yr cal BP may overestimate the age of deposition by thousands of years, if compared to the more reliable basal OSL age of AZ-W7 of *ca* 12 000 years. This OSL age, however, confirms the latest Pleistocene, pre-transgressive age of the dunes underlying the sabkha sequence, when sand dunes covered large parts of the entire dry Gulf (Sarnthein, 1972; Strohmenger & Jameson, 2015). The ^{14}C data derived from the deep wells of AZ-W6 and AZ-W7 show multiple inconsistencies and generally cover the age range of the earlier part of the mid-Holocene RSL highstand only. They are not in accordance with the consistent chronostratigraphy of the vibracores. Reasons may include longshore reworking of dated *Cerithium* shells along the outer barrier and possible incorporation into deeper parts of the well through the coring process. Thus, age data of AZ-W6 and AZ-W7 were not considered for the model of sabkha formation.

The OSL ages show relatively low precision due to low dose rates (0.6 to 1.1 Gy ka^{-1}) and spatially heterogeneous beta radiation in the heterogeneous coastal sediments dominated by quartz and different carbonate, similar to that experienced by Brill *et al.* (2017). Thus, for the aeolian (Facies E2) and low-energy foreshore (Facies F2) sediments from AZ-T1 and AZ-W7, which show no indication of incomplete OSL signal resetting in their D_e distributions, large aliquots of 8 mm diameter in combination with the CAM reduce the influence of spatial dose-rate variability and increase OSL signal intensities. The higher-energetic foreshore deposits (Facies F1) of AZ-T2, in contrast, show clear indication of incomplete OSL signal resetting in their D_e distributions. Smaller 2 mm aliquots combined with the MAM for burial-dose determination were applied to account for these effects. The resulting OSL ages are in stratigraphic order and either agree with (seaward part of AZ-T2) or are significantly younger than ^{14}C-AMS ages from similar strata, which are prone to reworking. Thus, the OSL data are considered to provide robust chronologies for sediment deposition of all dated facies.

Sabkha formation in space and time

During MIS stages 4 to 2, the Arabian Gulf was a large river valley draining the Euphrates and Tigris basin and receiving numerous tributaries from the Iranian landmass (short, steep gradient) and the Arabian Shield (longer, low gradient). The pre-transgressive (before 14 000 to 12 000 years ago) sedimentation inside the Gulf was dominated by fluvial and aeolian quartz sand and silt (Sarnthein, 1972; Stoffers & Ross, 1979; Ross *et al.*, 1986; Strohmenger & Jameson,

2015). In the marginal Gulf of Salwa, barchanoid dunes dominated under a presumably hyperarid climate regime before the onset of the Holocene (Al-Hinai *et al.*, 1987; Goudie *et al.*, 2000; Leighton *et al.*, 2014) and the transgression, respectively (Fig. 16A). Massive gypsum (Facies A) at the base of AZ-W6 (Figs 9 and S2) indicates the localized formation of a pre-transgressive sabkha or saline lake inside an interdunal depression.

Based on the few systematically dated and published RSL index points of the mid-Holocene RSL highstand in Qatar (Vita-Finzi, 1978; Engel & Brückner, 2014; Rivers *et al.*, 2020), rising RSL reached present-day levels around 6500 years ago – 1000 years later than estimated in Puls *et al.* (2009) and Billeaud *et al.* (2014). At that time, the area of the sabkha of Al-Kharayej became flooded and a narrow beach started to form (Figs 16B and 17). At the time of the highstand, *ca* 6000 years ago (Strohmenger & Jameson, 2015; Rivers *et al.*, 2020), a flying spit started to grow from the beach to form the nucleus of the later broad outer barrier.

At 5500 to 5000 cal yr BP, the main spit diverted landward, developed a snaky outline and started to enclose the northern section of today's sabkha (Figs 16C and 17). Thus, the northern section quickly evolved from open-coast to open-lagoon and protected-lagoon conditions within *ca* 1000 years. Deviations of spits have been observed in various coastal settings elsewhere, but whether they are triggered by major storms or thresholds in the feedback between the production and distribution of sediment and substrate morphology (Kwarteng *et al.*, 2005) is difficult to decipher, even though it was previously found that spit curvature is linked to wave-energy reduction (Allard *et al.*, 2008). Small-scale cuspate spits along both sides of the snaky spit (Fig. 14) indicate a longshore drift towards the south-east on the southern side and – less distinct – towards the north-west on the northern, inner side, where it was possibly driven by tidal currents. These diverging mechanisms forming the spit on both sides might have led to its snaky outline. The entire spit until this time had grown by a rate of *ca* 2.5 to 3.0 m yr^{-1}.

At 4500 to 4000 cal yr BP, the snaky barrier had nearly constrained the northern sabkha section. The closed lagoon gradually filled with clastic deposits, skeletal grains and evaporites from south to north, driven by the tidal current entering from the south and indicated by accretionary, curved shorelines visible in Fig. 14 ('linear accretion features'). Meanwhile, the spit of the outer barrier had grown further south increasing the area of protected-lagoon conditions in today's main sabkha section (Fig. 16D). An increase of evaporation rates supporting the further transformation into a salina and sabkha later on can be inferred from significant aridization trends after the early to mid-Holocene humid phase across the Arabian Peninsula (Fleitmann *et al.*, 2003; Parker *et al.*, 2016; Engel *et al.*, 2017, 2020). Shallowing of the entire coastal geomorphic system was driven by both gradual coastal and aeolian sedimentation and the initiation of the RSL fall at that time (cf. Parker *et al.*, 2020). The RSL-related lowering of the capillary fringe in the supratidal sabkha of the northern section resulted in deflation (cf. Fryberger *et al.*, 1988), which has also been observed in the landward part of sabkhas elsewhere in Qatar (Strohmenger & Jameson, 2015) and the karst basin of Asaila close to the Gulf of Salwa coast (Engel *et al.*, 2020). A gradual reduction of aeolian sand supply and sand movement in the form of barchanoid dunes within the Shamal corridor, which is roughly shore-parallel at the study site, has to be expected as the transgression had cut off the upwind sand source inside the Bahrain Ridge and the Gulf of Salwa, leading to long-term deprivation of sand on the entire peninsula (Embabi & Ashour, 1993; Engel *et al.*, 2018).

At 3500 to 3000 cal yr BP, the tidal connection had closed and a salina had formed, gradually transitioning into a supratidal sabkha. Rapid progradation of the outer spit (*ca* 6 m yr^{-1} since 5500 to 5000 cal yr BP) was fuelled by RSL fall (cf. Nielsen & Johannessen, 2008) and led to the extension of the open lagoon south of the snaky barrier. At the same time, the main spit accreted westward and widened. Several potential small-scale tidal inlets and tidal deltas cutting the older part of the spit can be identified in the satellite image (Fig. 14). In the northern part of this lagoon, conditions became increasingly protected, while at the northernmost margin the sabkha started to form (Fig. 16E). Beach ridge-type features identifiable on satellite imagery and between the inner boundary of the main spit and the deviating snaky spit, labelled as 'linear accretion features' in Fig. 14, reflect contraction of the protected lagoon. Whether these features correspond to beach ridges or cheniers (Shinn, 1973a, 2011), as they are underlain and flanked by muddy lagoonal facies (cf. Otvos, 2000), is difficult to infer, because they were not morphologically visible in the field.

At 2000 to 1500 cal yr BP, the main spit had almost reached the modern shape of the outer barrier constraining the sabkha. A tidal connection in the south was still open permitting limited exchange of water (Fig. 16F). The inner part of this closed lagoon, as reflected by AZ-W5, subsequently developed into a salina, before the closure of the barrier in the south led to present-day supratidal sabkha conditions (Figs 16G and 17). Further lowering of the Stokes surface resulted in deflation over the last two millennia, even though these effects are not as severe as in the northern section (Fig. 10).

Based on this spatio-temporal reconstruction, the sabkha of Al-Kharayej is a suitable example for a longshore transport-driven, spit-controlled formation, as systematically outlined by Purser (1985). Along the north-eastern coast of Qatar, however, similar lagoons are not yet entirely closed off (Shinn, 1973a; Billeaud *et al.*, 2014). The sabkha of Al-Kharayej stands in genetic contrast to the Mesaieed sabkha in the south-east of Qatar (Strohmenger & Jameson, 2015), which formed mainly due to coastal progradation fed by high detrital input of 'calving' barchan dunes in combination with evaporite pumping and the infiltration of seawater (Shinn, 1973b). Furthermore, it does not entirely comply with the classical model of sabkha formation as developed along the UAE coast, where the shore-perpendicular accumulation of coastal deposits during high tides or storms in combination with the mid-Holocene to late Holocene RSL fall results in the progradation of wide, low-inclination tidal flats into the lagoons and the precipitation of interstitial evaporites in the supratidal zone (Evans, 2011).

The regressive sabkha sequence of AZ-W5 in the centre of the main sabkha, showing by far the highest concentration of halite, supports the bull's eye model, describing the concentric sequence of different evaporitic minerals depending on their solubility. According to the contraction of the lagoon and salina from the margins to the centre, the mineral of highest solubility, i.e. halite, is dominant in the centre, followed by gypsum and carbonates towards the margins (Warren *et al.*, 1985; Sonnenfeld & Perthuisot, 1989; Ginau *et al.*, 2012).

Diagenetic modification of the sabkha: implications for reservoir characteristics

Many of the oil and gas reservoirs in the Middle East formed under conditions similar to the mid-Holocene to late Holocene coastal progradation along the coastline of Qatar. Sabkha sequences, such as the one described here, represent baffles or seals in the sedimentary record, due to the abundance of porosity-destroying evaporites (Strohmenger & Jameson, 2015). After burial, the primary precipitated gypsum will be transformed to anhydrite-after-gypsum, forming efficient barriers or seals, depending on the lateral and vertical continuity and thickness. Thus, the sabkha of Al-Kharayej represents a modern analogue for depositional and diagenetic processes controlling reservoir property and quality of the arid-climate carbonates, represented by the Permo-Triassic Khuff and the Jurassic Arab formations, even though its siliciclastic content is higher than in the fossil examples. Based on the main controlling factors driving coastal sedimentation – some of which equally affect the entire peninsula (RSL; climate), whereas others are site-specific (coastline orientation; wind, wave and tidal energy; depositional relief; sediment sources) – coastal sedimentation patterns in Qatar can be separated into windward, leeward, oblique and protected sections (Strohmenger & Jameson, 2015).

For instance, the oblique coastal system of the Mesaieed sabkha (south-east Qatar), characterized by an upper, middle and lower sabkha, as well as the coastal area, all evolving since *ca* 8000 years ago, differs from Al-Kharayej. While the upper and middle sabkha lithosomes show signs of significant deflation and diagenetic overprinting through gypsum precipitation (especially laminated and buckled gypsum crust in the upper part), the lower sabkha and coastal area consist of a series of prograding spits of coarse skeletal material with surprisingly grainy facies in the associated back-beach-lagoon and tidal-flat environments (Strohmenger & Jameson, 2015).

The sabkha of Al-Kharayej also experiences longshore sediment transport, but under lower wave and tidal-energy conditions and a shore-parallel main wind direction. In contrast to the sabkha of Mesaieed, where the Shamal wind drives the longshore current away from the coast in an oblique angle, forcing a sequence of spits to prograde into the Gulf, at Al-Kharayej only one major spit made up of coarse skeletal and quartz sand formed. Furthermore, there is a relatively porous section of dune sands of unknown thickness between the transgressive marine to coastal wedge of the sabkha and the Eocene bedrock, which has not been described at Mesaieed (Strohmenger & Jameson, 2015). At Al-Kharayej, the majority of the sabkha lithosome consists of mid-energy open to protected lagoon facies

(Facies D1, C2, C1), i.e. carbonate mud with varying amounts of skeletal debris, ooids and other grainy particles. These facies reach a thickness of up to 6 m in the centre (for example, AZ-W11) and up to 15 m beneath the outer barrier (AZ-W6), where open-lagoon packstone dominates. Interestingly, laminated gypsum crust, interpreted as subaqueous gypsum precipitation during folding of lower-lying parts of the sabkha (Strohmenger & Jameson, 2015), has not been observed, while buckled gypsum crust (Facies A), related to gypsum growth within pores of the sediment column through capillary rise of saline groundwater or seawater (Strohmenger & Jameson, 2018), is very common throughout the uppermost layer in varying intensity. This type of diagenetic overprinting, along with the concentrated swallow-tail, salina-type gypsum crystals found in the uppermost layers of the central area around AZ-W5 (Facies B), is restricted to the upper few decimetres of the sediment column (14 cm in AZ-W10; 24 cm in AZ-W5). While dolomite is a major component of many other sabkha sequences in Qatar and Abu Dhabi (Bontognali *et al.*, 2010; Strohmenger *et al.*, 2010, 2011; Brauchli *et al.*, 2016; Shalev *et al.*, 2021), only minor amounts were found at Al-Khareyej. This coincides with a lack of thick and continuous microbial deposits, which are also prominent features throughout many other costal sabkha sequences along the southern Arabian Gulf.

Al-Kharayej represents a model of a complex, heterogeneous reservoir system, deposited under relatively low wave-energy and tidal-energy conditions. In the absence of stepwise seaward migration of coarse-grained beaches and spits, as in Mesaieed, finer-grained carbonate-mud facies dominates the area behind the main barrier. Secondary, but still very early diagenetic plugging of the pore space by gypsum, as observed at Mesaieed (up to 60% of the porosity is lost by gypsum cementation within the upper sabkha environment; Strohmenger & Jameson, 2015), is less intense in the study area. In summary, the sedimentary architecture of Al-Kharayej is quite unique along the Qatar coastline and not only differs from the one in Mesaieed, but also from the windward coast at Al-Ruwais, dominated by Holocene carbonates (beaches, aeolian dunes, and coral reefs/patch reefs; Purkis *et al.*, 2017; Rivers *et al.*, 2020), the eastern, oblique coastline at Al-Dakhirah, dominated by longshore transported carbonates (Billeaud *et al.*, 2014), and the south-eastern, leeward coastline at Khor Al-Adaid, dominated by siliciclastic aeolian dunes and evaporites (sabkha-type gypsum; Rivers *et al.*, 2019b).

CONCLUSIONS

Coastal sabkha formation in Qatar is driven by regional [relative sea-level (RSL) changes; climate] and local (coastline orientation; wind, wave and tidal energy, longshore drift; depositional relief; sediment sources) factors. Among these, RSL changes are the main driver of the general pattern of early to mid-Holocene transgression and subsequent regression, leading to coastal progradation and the formation of narrow beach-ridge sequences (for example, Al-Sirriyah; Engel & Brückner, 2014), wider spit sequences with tidal flats in between (for example, Mesaieed; Strohmenger & Jameson, 2015) or various forms of coastal sabkhas, such as at the protected coast of Al-Kharayej.

At Al-Kharayej, the coastline runs roughly parallel to the Shamal winds causing a mainly oblique angle of approaching waves. This in combination with a low to mid-energy wave regime, a low tidal range, as well as abundant sediment available in the Gulf of Salwa through reworking of drowned dunes and the authigenic production of skeletal carbonates led to the formation of a large coastal sabkha above the pre-transgressive, Pleistocene dune surface. Fifteen different facies types were identified from 12 sediment cores and two trenches. The sabkha's parasequence comprises pre-transgressive dune sands (Facies E2), a thin, transgressive layer of reworked dune material (Facies E1), a mid-energy open-coast to open-lagoon facies (Facies D1), overlain by a low-energy lagoonal facies (Facies C1, C2), closed lagoon to salina (Facies B) and, finally, the supratidal sabkha diagenetic overprint (Facies A).

In combination with the ^{14}C and optically stimulated luminescence (OSL) dataset, marine flooding of the area resulted in open-coast to open-lagoonal sedimentation and the formation of a beach at its landward margin. Initial spit formation at the very northern end can be reconstructed for the transition from the mid-Holocene transgression to RSL highstand, around 6000 cal yr BP. During the following millennium, this main outer spit prograded southward and a snaky, low-energy spit diverted landward, gradually closing off a lagoon in the northern part of the sabkha around 4500 to 4000 cal yr BP. The falling RSL and longshore

drift resulted in further southward extension and widening of the outer spit as well as shallowing of the open lagoon south of the snaky barrier. Around 2000 to 1500 cal yr BP, the outer spit had almost reached its current shape, gradually closing the landward lagoon, leading to salina and, finally, sabkha conditions. This almost complete separation of the lagoon from the Gulf of Salwa caused the formation of a back-barrier salina (saline lake), where subaqueous prismatic gypsum precipitated in the form of gypsum swallow-tail crystals (Figs 5, 8C and 8D). After drying out, the salina deposits were thinly covered by aeolian sand and overprinted under sabkha conditions. In some parts, deflation led to the erosion of the uppermost layer.

In contrast to most other sabkhas described in literature, such as the famous examples along the United Arab Emirates coast (e.g. Alsharhan & Kendall, 2003; Evans, 2011), sabkha genesis at Al-Khareyej mainly results from the longshore drift and sediment availability nurturing a spit system that creates a protected, shallowing lagoon. In combination with RSL fall after the mid-Holocene highstand, this low-energy environment dominated by carbonate muds silted up and transformed into a supratidal coastal sabkha. This is also in contrast to the east coast of Qatar, for example, the coarser-grained Mesaieed sabkha, as grainstone facies at Al-Khareyej is mostly restricted to the main outer barrier and the thinner and narrower snaky barrier. Diagenetic overprinting is mostly present in the form of a buckled gypsum crust (sabkha-type gypsum and minor salt precipitation within the upper centimetres of the sediment). Unlike at Mesaieed, where extensive early diagenetic gypsum precipitation significantly reduced the pore space, plugging of the pore space by gypsum cementation has a less intense impact on reservoir properties at Al-Kharayej.

ACKNOWLEDGEMENTS

The authors thank ExxonMobil Research Qatar and ExxonMobil Upstream Integrated Solutions for the permission to publish this paper. The work of ME was further supported by funds obtained through a Max Delbrück Prize, junior category, awarded by the University of Cologne in 2014 (ZUK 81/1). For valuable discussions we thank John M. Rivers (ExxonMobil Research Qatar). Numerous comments and suggestions by the editors Peir Pufahl and Gregor Eberli, as well as Peter Homewood, Tomaso Bontognali, Chris Kendall and one anonymous reviewer are gratefully acknowledged and greatly helped to improve the manuscript. Open Access funding enabled and organized by Projekt DEAL.

DATA AVAILABILITY STATEMENT

Data from this paper can be made available by the authors upon reasonable request.

REFERENCES

Ahmed, M.A.-O.S. (1991) Recent benthic foraminifers from Tarut Bay, Arabian Gulf coast of Saudi Arabia. *J. Micropalaeontol.*, **10**, 33–38.

AI-Abdul-Razzaq, S.K., **Shublaq, W.** and **Al-Sheikh, Z.** (1982) Ostracode distribution and ecology of Sulaibikhat Bay, Kuwait. *Mar. Geol.*, **47**, 57–75.

Al-Abdul-Razzaq, S., **Shublaq, W.** and **Al-Sheikh, Z.** (1983) The marine benthic microfauna of the tidal flats of Kuwait. *J. Univ. Kuwait Sci.*, **10**, 101–110.

Al-Farraj, A. (2005) An evolutionary model for Sabkha development on the north coast of the UAE. *J. Arid Environ.*, **63**, 740–755.

Al-Hinai, K.G., **McMahon Moore, J.** and **Bush, P.R.** (1987) LANDSAT image enhancement study of possible submerged sand-dunes in the Arabian Gulf. *Int. J. Remote Sens.*, **8**, 251–258.

Al-Hitmi, H.H. (2000) Recent benthic Foraminifera from the local water of Qatar, Arabian Gulf. *Qatar Univ. Sci. J.*, **20**, 167–179.

Al-Jaloud, A.A. and **Hussain, G.** (2006) Sabkha ecosystem and halophyte plant communities in Saudi Arabia. In: *Sabkha Ecosystems: Volume II: West and Central Asia* (Eds Ajmal Khan, M., Böer, B., Kust, G.S. and Barth, H.-J.), pp. 1–7. Springer, Dordrecht.

Al-Kahtany, K., **Youssef, M.** and **El-Sorogy, A.** (2015) Geochemical and foraminiferal analyses of the bottom sediments of Dammam coast, Arabian Gulf, Saudi Arabia. *Arab. J. Geosci.*, **8**, 11121–11133.

Allard, J., **Bertin, X.**, **Chaumillon, E.** and **Pouget, F.** (2008) Sand spit rhythmic development: A potential record of wave climate variations? Arçay Spit, western coast of France. *Mar. Geol.*, **253**, 107–131.

Alsharhan, A.S. and **Kendall, C.G.St.C.** (2003) Holocene coastal carbonates and evaporites of the southern Arabian Gulf and their ancient analogues. *Earth Sci. Rev.*, **61**, 191–243.

Alsharhan, A.S. and **Kendall, C.G.S.C.** (2011) Introduction to Quaternary carbonate and evaporite sedimentary facies and their ancient analogues. In: *Quaternary Carbonate and Evaporite Sedimentary Facies and their Ancient Analogues: A Tribute to Douglas James Shearman* (Eds Kendall, C.G.S.C., Alsharhan, A.S., Jarvis, I. and Stevens, T.), *IAS Spec. Publ.*, **43**, 1–10.

Al-Yousef, M. (2003) *Mineralogy, Geochemistry and Origin of Quaternary Sabkhas in the Qatar Peninsula, Arabian Gulf*. Doctoral thesis, University of Southampton, Southampton.

Arslan, M., **Kaminski, M.A.**, **Tawabini, B.S.**, **Ilyas, M.** and **Frontalini, F.** (2016) Benthic foraminifera in sandy

(siliciclastic) coastal sediments of the Arabian Gulf (Saudi Arabia): a technical report. *Arab. J. Geosci.*, **9**, 285.

Barth, H.-J. (1998) Sebkhas als Ausdruck von Landschaftsdegradation im zentralen Küstentiefland der Ostprovinz Saudi-Arabiens. *Regensburger Geogr. Schr.*, **29**, 1–279.

Bate, R.H. (1971) The distribution of recent ostracoda in the Abu Dhabi Lagoon, Persian Gulf. *Bull. Centre Rech. Pau – SNPA*, **5**, 239–256.

Bate, R.H. and **Gurney, A.** (1981) The ostracod genus *Loxoconcha* Sars from Abu Dhabi lagoon and the neighbouring near-shore shelf, Persian Gulf. *Bull. Br. Mus. Nat. Hist. (Zool.)*, **41**, 235–251.

Billeaud, I., **Caline, B.**, **Livas, B.**, **Tessier, B.**, **Davaud, E.**, **Frebourg, G.**, **Hasler, C.A.**, **Laurier, D.** and **Pabian-Goyheneche, C.** (2014) The carbonate-evaporite lagoon of Al-Dakhirah (Qatar): an example of a modern depositional model controlled by longshore transport. In: *Sedimentary Coastal Zones from High to Low Latitudes: Similarities and Differences* (Eds Martini, I.P. and Wanless, H.R.), *Geol. Soc. London Spec. Publ.*, **388**, 561–587.

Blott, S.J. and **Pye, K.** (2001) GRADISTAT: a grain size distribution and statistics package for the analysis of unconsolidated sediments. *Earth Surf. Proc. Landf.*, **26**, 1237–1248.

Bontognali, T.R., **Vasconcelos, C.**, **Warthmann, R.J.**, **Bernasconi, S.M.**, **Dupraz, C.**, **Strohmenger, C.J.** and **McKenzie, J.A.** (2010) Dolomite formation within microbial mats in the coastal sabkha of Abu Dhabi (United Arab Emirates). *Sedimentology*, **57**, 824–844.

Brauchli, M., **McKenzie, J.A.**, **Strohmenger, C.J.**, **Sadooni, F.**, **Vasconcelos, C.** and **Bontognali, T.R.** (2016) The importance of microbial mats for dolomite formation in the Dohat Faishakh sabkha, Qatar. *Carbonate. Evaporite.*, **31**, 339–345.

Brill, D., **May, S.M.**, **Shah-Hosseini, M.**, **Rufer, D.**, **Schmidt, C.** and **Engel, M.** (2017) Luminescence dating of cyclone-induced washover fans at Point Lefroy (NW Australia). *Quat. Geochronol.*, **41**, 134–150.

Butler, G.P. (1969) Modern evaporite deposition and geochemistry of coexisting brines, the Sabkha, Trucial coast, Arabian Gulf. *J. Sediment. Petrol.*, **39**, 70–89.

Chao, S.-Y., **Kao, T.W.** and **Al-Hajri, K.R.** (1992) A numerical investigation of circulation in the Arabian Gulf. *J. Geophys. Res.*, **97**, 11219–11236.

Cuttler, R. and **Al-Naimi, F.A.** (2013) From land-locked desert to maritime nation: Landscape evolution and taphonomic pathways in Qatar from 14 ka. *Adumatu*, **28**, 7–22.

Dashtgard, S.E., **MacEachern, J.A.**, **Frey, S.E.** and **Gingras, M.K.** (2012) Tidal effects on the shoreface: Towards a conceptual framework. *Sediment. Geol.*, **279**, 42–61.

Davis, R.A. (1978) Beach and nearshore zone. In: *Coastal Sedimentary Environments* (Ed. Davis, R.A.), pp. 237–285. Springer, New York, NY.

Dietze, E. and **Dietze, M.** (2019) Grain-size distribution unmixing using the R package EMMAgeo. *E&G Quaternary Sci. J.*, **68**, 29–46.

Embabi, N.S. and **Ashour, M.M.** (1993) Barchan dunes in Qatar. *J. Arid Environ.*, **25**, 49–69.

Engel, M., **Boesl, F.** and **Brückner, H.** (2018) Migration of barchan dunes in Qatar—controls of the Shamal, teleconnections, sea-level changes and human impact. *Geosciences*, **8**, 240.

Engel, M. and **Brückner, H.** (2014) The South Qatar Survey Project (SQSP) – Preliminary findings on Holocene coastal changes and geoarchaeological archives. *Z. Orient-Archäol.*, **7**, 290–301.

Engel, M., **Matter, A.**, **Parker, A.G.**, **Parton, A.**, **Petraglia, M.D.**, **Preston, G.W.** and **Preusser, F.** (2017) Lakes or wetlands? A comment on 'The middle Holocene climatic records from Arabia: Reassessing lacustrine environments, shift of ITCZ in Arabian Sea, and impacts of the southwest Indian and African monsoons' by Enzel et al. *Global Planet. Change*, **148**, 258–267.

Engel, M., **Rückmann, S.**, **Drechsler, P.**, **Brill, D.**, **Opitz, S.**, **Fassbinder, J.**, **Pint, A.**, **Peis, K.**, **Wolf, D.**, **Gerber, C.**, **Pfeiffer, K.**, **Eichmann, R.** and **Brückner, H.** (2020) Sediment-filled karst depressions and *riyad* – key archaeological environments of south Qatar. *E&G Quaternary Sci. J.*, **68**, 215–236.

Evans, G. (2011) An historical review of the Quaternary sedimentology of the Gulf (Arabian/Persian Gulf) and its geological impact. In: *Quaternary Carbonate and Evaporite Sedimentary Facies and their Ancient Analogues: A Tribute to Douglas James Shearman* (Eds Kendall, C.G.S.C., Alsharhan, A.S., Jarvis, I. and Stevens, T.), *IAS Spec. Publ.*, **43**, 11–44.

Evans, G., **Schmidt, V.**, **Bush, P.** and **Nelson, H.** (1969) Stratigraphy and geologic history of the sabkha, Abu Dhabi, Persian Gulf. *Sedimentology*, **12**, 145–159.

Farr, T.G., **Rosen, P.A.**, **Caro, E.**, **Crippen, R.**, **Duren, R.**, **Hensley, S.**, **Kobrick, M.**, **Paller, M.**, **Rodriguez, E.**, **Roth, L.**, **Seal, D.**, **Shaffer, S.**, **Shimada, J.**, **Umland, J.**, **Werner, M.**, **Oskin, M.**, **Burbank, D.** and **Alsdorf, D.** (2007) The Shuttle Radar Topography Mission. *Rev. Geophys.*, **45**, RG2004.

Feulner, G. and **Hornby, R.J.** (2006) Intertidal molluscs in UAE lagoons. *Tribulus*, **16**(2), 17–23.

Fleitmann, D., **Burns, S.J.**, **Mangini, A.**, **Mudelsee, M.**, **Kramers, J.**, **Villa, I.**, **Neff, U.**, **Al-Subbary, A.A.**, **Buettner, A.**, **Hippler, D.** and **Matter, A.** (2007) Holocene ITCZ and Indian monsoon dynamics recorded in stalagmites from Oman and Yemen (Socotra). *Quaternary Sci. Rev.*, **26**, 170–188.

Fryberger, S.G., **Schenk, C.J.** and **Krystinik, L.F.** (1988) Stokes surfaces and the effects of near-surface groundwater-table on aeolian deposition. *Sedimentology*, **35**, 21–41.

Galbraith, R.F., **Roberts, R.G.**, **Laslett, G.M.**, **Yoshida, H.** and **Olley, J.M.** (1999) Optical dating of single grains of quartz from Jinmium rock shelter, northern Australia, Part I: experimental design and statistical models. *Archaeometry*, **41**, 339–364.

Ginau, A., **Engel, M.** and **Brückner, H.** (2012) Holocene chemical precipitates in the continental sabkha of Tayma (NW Saudi Arabia). *J. Arid Environ.*, **84**, 26–37.

Goudie, A.S., **Colls, A.**, **Stokes, S.**, **Parker, A.**, **White, K.** and **Al-Farraj, A.** (2000) Latest Pleistocene and Holocene dune construction at the north-eastern edge of the Rub Al Khali, United Arab Emirates. *Sedimentology*, **47**, 1011–1021.

Gunatilaka, A., **Al-Temeemi, A.**, **Saleh, A.** and **Nassar, N.** (1985) A new occurrence of bassanite in recent evaporitic environments, Kuwait, Arabian Gulf. *Kuwait J. Sci.*, **12**, 157–166.

Hammer, Ø., **Harper, D.A.** and **Ryan, P.D.** (2001) PAST: paleontological statistics software package for education and data analysis. *Palaeontol. Electron.*, **4**, 4.

Homewood, P., **Vahrenkamp, V.**, **Mettraux, M.**, **Mattner, J.**, **Vlaswinkel, B.**, **Droste, H.** and **Kwarteng, A.** (2007) Bar Al Hikman: a modern carbonate and outcrop analogue in Oman for Middle East Cretaceous fields. *First Break*, **25**, 55–61.

Hsü, K.J. and **Siegenthaler, C.** (1969) Preliminary experiments on hydrodynamic movement induced by evaporation and their bearing on the dolomite problem. *Sedimentology*, **12**, 11–25.

Hughes Clarke, M.W. and **Keij, A.J.** (1973) Organisms as producers of carbonate sediment and indicators of environment in the southern Persian Gulf. In: *The Persian Gulf* (Ed. Purser, B.H.), pp. 33–56, Springer, Berlin.

Illing, L.V. and **Taylor, J.C.M.** (1993) Penecontemporaneous dolomitization in Sabkha Faishakh, Qatar: evidence from changes in the chemistry of the interstitial brines. *J. Sediment. Petrol.*, **63**, 1042–1048.

Jameson, J., **Puls, D.D.** and **Kozar, M.G.** (2009) Holocene sabkha and coastal systems of Qatar: Process models for the interpretation of ancient Arabian Plate carbonate evaporite reservoirs. In: International Petroleum Technology Conference, Doha, 7–9 December 2009. https://doi.org/10.2523/IPTC-13679-MS

Kassler, P. (1973) The structural and geomorphic evolution of the Persian Gulf. In: *The Persian Gulf* (Ed. Purser, B.H.), pp. 11–32, Springer, Berlin.

Kwarteng, A., **Homewood, P.** and **Mettraux, M.** (2005) Remote sensing of the modern carbonate system of the Bar Al Hikman Peninsula, Oman. In: *Proceedings. 2005 IEEE International Geoscience and Remote Sensing Symposium (IGARSS '05), 2005, Seoul*, pp. 1428–1431.

Lambeck, K. (1996) Shoreline reconstructions for the Persian Gulf since the last glacial maximum. *Earth Planet. Sci. Lett.*, **141**, 43–57.

Lambeck, K., **Rouby, H.**, **Purcell, A.**, **Sun, Y.** and **Sambridge, M.** (2014) Sea level and global ice volumes from the Last Glacial Maximum to the Holocene. *Proc. Natl. Acad. Sci.*, **111**, 15296–15303.

Leighton, C.L., **Bailey, R.M.** and **Thomas, D.S.G.** (2014) Interpreting and modelling late Quaternary dune accumulation in the southern Arabian Peninsula. *Quaternary Sci. Rev.*, **102**, 1–13.

Lokier, S.W., **Bateman, M.D.**, **Larkin, N.R.**, **Rye, P.** and **Stewart, J.R.** (2015) Late Quaternary sea-level changes of the Persian Gulf. *Quaternary Res.*, **84**, 69–81.

Mauz, B., **Vacchi, M.**, **Green, A.**, **Hoffmann, G.** and **Cooper, A.** (2015) Beachrock: a tool for reconstructing relative sea level in the far-field. *Mar. Geol.*, **362**, 1–16.

McKenzie, J.A., **Hsü, K.J.** and **Schneider, J.F.** (1980) Movement of subsurface waters under the sabkha, Abu Dhabi, UAE, and its relation to evaporative dolomite genesis. In: *Concepts and Models of Dolomitization* (Eds Zenger, D.H., Dunham, J.B. and Ethington, R.L.), *SEPM Spec. Publ.*, **28**, 11–30.

Mettraux, M., **Homewood, P.W.**, **Kwarteng, A.Y.** and **Mattner, J.** (2011) Coastal and continental sabkhas of Barr Al Hikman, Sultanate of Oman. *IAS Spec. Publ.*, **43**, 183–204.

Morris, S. and **Morris, N.** (1993) New shells from the UAE's east coast. *Tribulus*, **3**(1), 18–19.

Mostafawi, N. (2003) Recent ostracods from the Persian Gulf. *Senck. marit.*, **32**, 51–75.

Neal, A., **Pontee, N.I.**, **Pye, K.** and **Richards, J.** (2002) Internal structure of mixed-sand-and-gravel beach deposits revealed using ground-penetrating radar. *Sedimentology*, **49**, 789–804.

Nielsen, L.H. and **Johannessen, P.N.** (2008) Facies architecture and depositional processes of the Holocene-Recent accretionary forced regressive Skagen spit system, Denmark. *Sedimentology*, **56**, 935–968.

Otvos, E. (2000) Beach ridges – definitions and significance. *Geomorphology*, **32**, 83–108.

Parker, A.G., **Armitage, S.J.**, **Engel, M.**, **Morley, M.W.**, **Parton, A.**, **Preston, G.W.**, **Russ, H.** and **Drechsler, P.** (2020) Palaeoenvironmental and sea level changes during the Holocene in Eastern Saudi Arabia and their implications for Neolithic populations. *Quaternary Sci. Rev.*, **249**, 106618.

Parker, A.G., **Preston, G.W.**, **Parton, A.**, **Walkington, H.**, **Jardine, P.E.**, **Leng, M.J.** and **Hodson, M.J.** (2016) Low-latitude Holocene hydroclimate derived from lake sediment flux and geochemistry. *J. Quaternary Sci.*, **31**, 296–299.

Puls, D.D., **Jameson, J.**, **Kozar, M.**, **Al-Ansi, H.** and **LeBlanc, J.** (2009) The Dukhan Sabkha: a modern analog for the Arab C Carbonate Reservoir, Dukhan Field, Qatar. In: *International Petroleum Technology Conference, Doha, 7–9 December 2009*. https://doi.org/10.2523/IPTC-13629-MS

Purkis, S.J., **Rivers, J.**, **Strohmenger, C.J.**, **Warren, C.**, **Yousif, R.**, **Ramirez, L.** and **Riegl, B.** (2017) Complex interplay between depositional and petrophysical environments in Holocene tidal carbonates (Al Ruwais, Qatar). *Sedimentology*, **64**, 1646–1675.

Purser, B.H. (1985) Coastal evaporite systems. In: *Hypersaline Ecosystems – The Gavish Sabkha* (Eds Friedman, G.M. and Krumbein, W.E.), *Ecolog. Stud.*, **53**, 72–102.

Purser, B.H. and **Seibold, E.** (1973) The principal environmental factors influencing Holocene sedimentation and diagenesis in the Persian Gulf. In: *The Persian Gulf* (Ed. Purser, B.H.), pp. 1–9. Springer, Berlin.

Rao, P.G., **Al-Sulaiti, M.** and **Al-Mulla, A.H.** (2001) Winter shamals in Qatar, Arabian Gulf. *Weather*, **56**, 444–451.

Reinson, G.E. (1979) Facies Models 14. Barrier Island Systems. *Geosci. Can.*, **6**, 51–68.

Rivers, J., **Engel, M.**, **Dalrymple, R.**, **Yousif, R.**, **Strohmenger, C.J.** and **Al-Shaikh, I.** (2020) Are carbonate barrier islands mobile? Insights from a mid- to late-Holocene system, Al Ruwais, northern Qatar. *Sedimentology*, **67**, 534–558.

Rivers, J.M. and **Larson, K.P.** (2018) The Cenozoic kinematics of Qatar: evidence for high-angle faulting along the Dukhan 'anticline'. *Mar. Petrol. Geol.*, **92**, 953–961.

Rivers, J.M., **Skeat, S.L.**, **Yousif, R.**, **Liu, C.**, **Stanmore, E.**, **Tai, P.** and **Al-Marri, S.M.** (2019a) The depositional history of near-surface Qatar aquifer rocks and its impact on matrix flow and storage properties. *Arab. J. Geosci.*, **12**, 380.

Rivers, J.M., **Varghese, L.**, **Yousif, R.**, **Whitaker, F.F.**, **Skeat, S.L.** and **Al-Shaikh, I.** (2019b) The geochemistry of Qatar coastal waters and its impact on carbonate sediment chemistry and early marine diagenesis. *J. Sediment. Res.*, **89**, 293–309.

Ross, D.A., **Uchupi, E.** and **White, R.S.** (1986) The geology of the Persian Gulf–Gulf of Oman region: A synthesis. *Rev. Geophys.*, **24**, 537–556.

Sarnthein, M. (1972) Sediments and history of the postglacial transgression in the Persian Gulf and northwest Gulf of Oman. *Mar. Geol.*, **12**, 245–266.

Schwartz, R.K. (1982) Bedform and stratification characteristics of some modern small-scale washover sand bodies. *Sedimentology*, **29**, 835–849.

Seltrust Engineering Ltd (1980) *Qatar Geological Map, scale 1:100,000, sheet 3*. Doha, Qatar.

Shalev, N., **Bontognali, T.R.R.** and **Vance, D.** (2021) Sabkha dolomite as an archive for the magnesium isotope composition of seawater. *Geology*, **49**, 253–256.

Sheppard, C., **Al-Husiani, M.**, **Al-Jamali, F.**, **Al-Yamani, F.**, **Baldwin, R.**, **Bishop, J.**, **Benzoni, F.**, **Dutrieux, E.**, **Dulvy, N.K.**, **Durvasula, S.R.V.**, **Jones, D.A.**, **Loughland, R.**, **Medio, D.**, **Nithyanandan, M.**, **Pilling, G.M.**, **Polikarpov, I.**, **Price, A.R.G.**, **Purkis, S.**, **Riegl, B.**, **Saburova, M.**, **Namin, K.S.**, **Taylor, O.**, **Wilson, S.** and **Zainal, K.** (2010) The Gulf: A young sea in decline. *Mar. Pollut. Bull.*, **60**, 13–38.

Shinn, E.A. (1973a) Carbonate coastal accretion in an area of longshore transport, NE Qatar, Persian Gulf. In: *The Persian Gulf* (Ed. Purser, B.H.), pp. 179–191. Springer, Berlin.

Shinn, E.A. (1973b) Sedimentary accretion along the leeward, SE coast of Qatar peninsula, Persian Gulf. In: *The Persian Gulf* (Ed. Purser, B.H.), pp. 199–209. Springer, Berlin.

Shinn, E.A. (2011) Interplay between Holocene sedimentation and diagenesis, and implications for hydrocarbon exploitation: Return to the sabkha of Ras Said, Qatar. In: *Quaternary Carbonate and Evaporite Sedimentary Facies and their Ancient Analogues: A Tribute to Douglas James Shearman* (Eds Kendall, C.G.S.C., Alsharhan, A.S., Jarvis, I. and Stevens, T.), *IAS Spec. Publ.*, **43**, 133–148.

Sonnenfeld, P. and **Perthuisot, J.P.** (1989) *Brines and Evaporites*. American Geophysical Union, Washington, DC, 126 pp.

State of Qatar (Ed.) (1980) *Geological Map, 1:100,000*. State of Qatar, Industrial Development Technical Centre, Doha.

State of Qatar (Ed.) (2009) *Qatar Survey Manual*. Urban Planning & Development Authority/The Centre for GIS, Doha.

Stewart, J.R., **Aspinall, S.**, **Beech, M.**, **Fenberg, P.**, **Hellyer, P.**, **Larkin, N.**, **Lokier, S.W.**, **Marx, F.G.**, **Meyer, M.**, **Miller, R.**, **Rainbow, P.S.**, **Taylor, J.D.**, **Whittaker, J.E.**, **Al-Mehsin, K.** and **Strohmenger, C.J.** (2011) Biotically constrained palaeoenvironmental conditions of a mid-Holocene intertidal lagoon on the southern shore of the Arabian Gulf: evidence associated with a whale skeleton at Musaffah, Abu Dhabi, UAE. *Quaternary Sci. Rev.*, **30**, 3675–3690.

Stoffers, P. and **Ross, D.A.** (1979) Late Pleistocene and Holocene sedimentation in the Persian Gulf—Gulf of Oman. *Sediment. Geol.*, **23**, 181–208.

Strohmenger, C.J. and **Jameson, J.** (2015) Modern coastal systems of Qatar as analogues for arid climate carbonate reservoirs: improving geological and reservoir modelling. *First Break*, **33**(5), 41–50.

Strohmenger, C.J. and **Jameson, J.** (2018) Gypsum stromatolites from Sawda Nathil: relicts from a southern coastline of Qatar. *Carbonate. Evaporite.*, **33**, 169–186.

Strohmenger, C.J., **Al-Mansoori, A.**, **Al-Jeelani, O.**, **Al-Shamry, A.**, **Al-Hosani, I.**, **Al-Mehsin, K.** and **Shebl, H.** (2010) The sabkha sequence at Mussafah Channel (Abu Dhabi, United Arab Emirates): facies stacking patterns, microbial-mediated dolomite and evaporite overprint. *GeoArabia*, **15**, 49–90.

Strohmenger, C.J., **Shebl, H.**, **Al-Mansoori, A.**, **Al-Mehsin, K.**, **Al-Jeelani, O.**, **Al-Hosani, I.**, **Al-Shamry, A.** and **Al-Baker, S.** (2011) Facies stacking patterns in a modern arid environment: a case study of the Abu Dhabi sabkha in the vicinity of Al-Qanatir Island, United Arab Emirates. In: *Quaternary Carbonate and Evaporite Sedimentary Facies and their Ancient Analogues: A Tribute to Douglas James Shearman* (Eds Kendall, C.G.S.C., Alsharhan, A.S., Jarvis, I. and Stevens, T.), *IAS Spec. Publ.*, **43**, 149–182.

Sugden, W. (1963) The hydrology of the Persian Gulf and its significance in respect to evaporite deposition. *Am. J. Sci.*, **261**, 741–755.

Taylor, J.C.M. and **Illing, L.V.** (1969) Holocene intertidal calcium carbonate cementation, Qatar, Persian Gulf. *Sedimentology*, **12**, 69–107.

Vita-Finzi, C. (1978) Environmental History. In: *Qatar Archaeological Report – Excavations 1973* (Ed. De Cardi, B.), pp. 11–25. Oxford University Press, Oxford.

Warren, J.K. (1996) Evaporites, brines and base metals: what is an evaporite? Defining the rock matrix. *Aust. J. Earth Sci.*, **43**, 115–132.

Warren, J.K. and **Kendall, C.G.St.C.** (1985) Comparison of marine (subaerial) and salina (subaqueous) evaporites; modern and ancient. *Am. Assoc. Petrol. Geol. Bull.*, **69**, 1013–1023.

Weatherall, P., **Marks, K.M.**, **Jakobsson, M.**, **Schmitt, T.**, **Tani, S.**, **Arndt, J.E.**, **Rovere, M.**, **Chayes, D.**, **Ferrini, V.** and **Wigley, R.** (2015) A new digital bathymetric model of the world's oceans. *Earth Space Sci.*, **2**, 331–345.

Whitaker, F., **Didi-Ooi, S.M.**, **Jameson, J.** and **Strohmenger, C.J.** (2014) Origins of evaporites in a Holocene mixed clastic and carbonate coastal sabkha: preliminary hydrological and geochemical data from Mesaieed Sabkha, Qatar. International Petroleum Technology Conference, 22–24 January 2014, IPTC-17567-MS. https://doi.org/10.2523/IPTC-17567-MS

Wood, W.W., **Sanford, W.E.** and **Habshi, A.R.S.A.** (2002) Source of solutes to the coastal sabkha of Abu Dhabi. *Geol. Soc. Am. Bull.*, **114**, 259–268.

Wood, W.W., **Sanford, W.E.** and **Frape, S.K.** (2005) Chemical openness and potential for misinterpretation of the solute environment of coastal sabkhat. *Chem. Geol.*, **215**, 61–372.

Manuscript received 4 June 2020; revision 30 July 2021; revision accepted 4 August 2021

Supporting Information

Additional information may be found in the online version of this article:

Appendix S1. Detailed methods and supplementary data.